A Comparative Study of Homogeneous Nucleation Parameterizations, Part II. 3-D Model Application and Evaluation

Yang Zhang[1,*] Ping Liu[1,2], Xiao-Huan Liu[1,3], Mark Z. Jacobson[4], Peter H. McMurry[5], Fangqun Yu[6], Shaocai Yu[7], and Kenneth L. Schere[7]

[1]Department of Marine, Earth, and Atmospheric Sciences, North Carolina State University, Raleigh, NC, USA
[2]School of Environmental Science and Engineering, Shanghai Jiao Tong University, Shanghai, China
[3]Environment Research Institute, Shandong University, Jinan, China
[4]Department of Civil and Environmental Engineering, Stanford University, Stanford, CA, USA
[5] Department of Mechanical Engineering, University of Minnesota, Minneapolis, Minnesota, USA
[6] Atmospheric Sciences Research Center, State University of New York at Albany, Albany, NY, USA
[7]Atmospheric Modeling and Analysis Division, the U.S. EPA, Research Triangle Park, NC, USA

Abstract

Following the examination and evaluation of twelve nucleation parameterizations presented in the Part I paper, eleven of them representing binary, ternary, kinetic, and cluster-activated nucleation theories are evaluated in the U.S. Environmental Protection Agency (EPA) Community Multiscale Air Quality (CMAQ) modeling system version 4.4. The 12-28 June 1999 Southern Oxidants Study (SOS) episode is selected as a testbed to evaluate simulated particulate matter (PM) number and size predictions of CMAQ with different nucleation parameterizations. The evaluation shows that simulated domain-wide maximum $PM_{2.5}$ number concentrations with different nucleation parameterizations can vary by 3 orders of magnitude. All parameterizations overpredict (by a factor of 1.4 to 1.7) the total number concentrations of accumulation-mode PM; and significantly underpredict (by factors of 1.3 to 65.7) those of Aitken-mode PM, resulting in a net underprediction (by factors of 1.3 to 13.7) of the total number concentrations of $PM_{2.5}$ under a polluted urban environment at a downtown station in Atlanta. The predicted number concentrations for Aitken-mode PM at this site can vary by up to 3 orders of magnitude, and those for accumulation-mode PM can vary by up to a factor of 3.2, with the best predictions by the power law of Sihto et al. (2006) (NMB of -31.7%) and the worst predictions by the ternary nucleation parameterization of Merikanto et al. (2007) (NMB of -93.1%). The ternary nucleation parameterization of Napari et al. (2002) gives relatively good agreement with observations but for a wrong reason. The power law of Kuang et al. (2008) and the binary nucleation parameterization of Harrington and Kreidenweis (1998) give better agreement than the remaining parameterizations. All the parameterizations fail to reproduce the observed temporal variations of PM number, volume, surface area concentrations. The significant variation in the performance of these parameterizations is caused by their different theoretical bases, formulations, and dependence on temperature, relative humidity, and the ambient levels of H_2SO_4 and NH_3. The controlling processes are different for PM number, mass, and surface areas. At urban/rural locations, some PM processes (e.g., homogeneous nucleation) and/or vertical transport may dominate the production of $PM_{2.5}$ number, and emissions, or PM processes, or vertical transport or their combinations may dominate the production of $PM_{2.5}$ mass and surface area. Dry deposition or some PM processes such as coagulation may dominate $PM_{2.5}$ number loss, and horizontal and vertical transport, and cloud processes (e.g., cloud scavenging and wet deposition) may dominate the loss of $PM_{2.5}$ mass and surface area concentrations. Sensitivity simulations show that the PM number and size distribution predictions are most sensitive to prescribed emission fractions of Aitken and accumulation-mode PM and the assumed initial PM size distribution, in addition to different homogeneous nucleation parameterizations.

Keywords: nucleation parameterizations, $PM_{2.5}$ number size distribution, CMAQ evaluation, process analysis, sensitivity study, SOS, ARIES

*Corresponding author: Yang Zhang, Department of Marine, Earth, and Atmospheric Sciences, Campus Box 8208, NCSU, Raleigh, NC 27695; e-mail: yang_zhang@ncsu.edu

1. Introduction

Three-dimensional (3-D) modeling of particulate matter (PM) properties (e.g., mass, number, and size distribution) is a formidable task because of the complexity of its physical and chemical processes and the demand for large computational resources. While most 3-D air quality models can reproduce the mass concentrations of PM with an aerodynamic diameter less than or equal to 2.5 μm and 10 μm (i.e., $PM_{2.5}$ and PM_{10}) within ~50% of the measurements, accurately simulating particle number concentrations and size distributions remains challenging (Zhang et al., 2006; Zhang, 2008). Numerous global and regional modeling studies focused on particle mass concentrations. Fewer studies simulated particle number concentrations and size distributions on both global (e.g., Spracklen et al., 2005, 2006, 2007, 2008; Korhonen et al., 2008; Yu and Luo, 2009) and regional scales (e.g., Zhang et al., 2006, 2010a; Elleman and Covert, 2009a, b). Most aerosol models perform poorly for the particle number concentrations and size distributions for several reasons. For example, the horizontal grid resolution used in most regional models ($\geq$ 12 km) is too coarse to reproduce point-wise measurements including particle mass and number concentrations. The number of particle size sections or modes used in most models is often too coarse to resolve the particle number concentrations (e.g., Zhang et al., 2004; 2006) despite exceptions for some models (e.g., Jacobson et al., 1999; Yu and Luo, 2009). Assumptions in model inputs and treatments (e.g., assumed primary emission fractions and associated size distributions) and imperfect model treatments used in some models (e.g., the use of a fixed standard deviation for particle size distribution in simulating particle dynamic processes such as coagulation and condensation) usually lead to errors in simulated particle number concentrations and size distributions (Zhang et al., 1999, 2006, 2010a). Further, one of the large uncertainties in simulating PM number concentrations and size distributions lies in the model treatment of new particle formation processes due to various homogeneous nucleation mechanisms. Use of different nucleation parameterizations in 3-D models introduces significant uncertainties in the predicted $PM_{2.5}$ number production rates and number concentrations (Zhang et al., 1999, 2009a; Roth

et al., 2003; Lucas and Akimoto, 2006; Elleman and Covert, 2009a, b; Yu et al., 2010), which in turn affect visibility, aerosol optical properties, cloud condensation nuclei (CCN), and cloud droplet number concentrations (CDNC) (Malm, 1979; McMurry et al., 2005; Seinfeld and Pandis, 2006; Spracklen et al., 2008; Yu and Luo, 2009; Pierce and Adams, 2009; Kuang et al., 2009; Merikanto et al., 2009a; Zhang et al., 2009a).

Particles are simulated in the U.S. Environmental Protection Agency (EPA) Community Multiscale Air Quality (CMAQ) modeling system with three lognormally-distributed modes: Aitken, accumulation, and coarse modes (correspond to particles with diameters up to approximately 0.1 μm, between 0.1 and 2.5 μm, and between 2.5 and 10 μm, respectively, for mass distribution) (Binkowski and Roselle, 2003; Byun and Schere, 2006). CMAQ simulates major aerosol processes including thermodynamic equilibrium for both inorganic and organic PM, gas-to-particle conversion processes such as binary homogeneous nucleation of sulfuric acid and water vapor, and condensation of gases on preexisting particles and dissolution of gases into cloud droplets, additional PM growth via coagulation, PM production via aqueous-phase chemistry, aerosol scavenged by cloud droplets, and dry and wet deposition. A number of changes have been made in the aerosol dynamic and thermodynamic treatments in CMAQ in the past few years as newer versions are released for public use. While those changes are targeted primarily at improving predictions of aerosol mass concentrations, the model's capability in simulating number concentration and size distribution remains unchanged due mainly to the use of the same homogeneous nucleation parameterization in version 4.4 and newer (although an improved treatment for PM mass concentrations may also help improve the accuracy of PM size distribution). The binary nucleation parameterization of Kulmala et al. (1998) is used as a default module in CMAQ version 4.4 and newer to simulate new particle formation. The parameterization of Harrington and Kreidenweis (1998) was used as a default module in the older versions of CMAQ (Binkowski and Roselle, 2003). The parameterization of Kulmala et al. (1998) was derived based on the classic binary nucleation theory. It predicts binary nucleation

103 rates up to 2-3 orders of magnitude lower than those predicted by its updated version (i.e., Vehkamäki
104 et al., 2002) due to the fact that its derivation contains mistakes in the kinetic treatment for hydrate
105 formation as pointed out by Vehkamäki et al. (2002) and Noppel et al. (2002). Park et al. (2006)
106 reported that the CMAQ-predicted $PM_{2.5}$ number concentrations with the parameterization of
107 Kulmala et al. (1998) were lower by a factor of 1000 than observations in the southeastern U.S.
108 Elleman and Covert (2009a) compared the CMAQ-predicted number concentrations for Aitken-mode
109 PM with observations obtained for the Pacific Northwest U.S. and found that CMAQ with the
110 parameterization of Kulmala et al. (1998) underpredicted the PM number concentrations by a factor
111 of 10-100.

112 Following the examination and evaluation of twelve nucleation parameterizations presented in
113 the Part I paper (Zhang et al., 2010b), nine nucleation parameterizations have been implemented into
114 CMAQ version 4.4 in this work to future study the sensitivity of simulated particle number
115 concentrations from 3-D CMAQ. These include four binary homogeneous nucleation (BHN)
116 parameterizations (i.e., Pandis et al. (1994), Fitzgerald et al. (1998), Vehkamäki et al. (2002), and Yu
117 (2008), referred to as PA94, FI98, VE02, YU08, respectively), three ternary homogeneous nucleation
118 (THN) parameterizations (i.e., Napari et al. (2002), Merikanto et al. (2007) with corrections in
119 Merikanto et al. (2009b), and Yu (2006), referred to as NA02, ME07, and YU06, respectively), and
120 two power laws representing empirical kinetic or cluster-activated nucleation (i.e., Sihto et al. (2006)
121 and Kuang et al. (2008), referred to as SI06 and KU08, respectively). The nine parameterizations are
122 evaluated along with two existing BHN parameterizations in CMAQ (i.e., Kulmala et al. (1998) and
123 Harrington and Kreidenweis (1998), referred to as KU98 and HK98, respectively) through their
124 applications to the summer 1999 Southern Oxidants Study (SOS99) episode. The parameterization of
125 Wexler et al. (1994) is examined in the Part I paper but excluded from the 3-D CMAQ application
126 here, because it exceeds the upper limits of nucleation rates under most atmospheric conditions
127 (Zhang et al., 2010b). While KU98 and NA02 are also not recommended for 3-D model applications

128 in the Part I paper, they have been used in several recent 3-D model applications. In particular, NA02
129 gives a seemingly good agreement (e.g., Gaydos et al., 2005; Jung et al., 2008, 2010; Elleman et al.,
130 2009b) and may be continuously used in the community. On the other hand, as indicated by Anttila
131 et al. (2005) and Merikanto et al. (2007), the derivation of this parameterization neglected the
132 ammonium bisulfate formation which governs the ternary nucleation process according to the
133 classical theory and such an omission leads to unrealistically high nucleation rates. NA02 is therefore
134 included in this study to evaluate whether it also gives a good agreement with PM number and size
135 distributions observations in the southeastern U.S. If this is true, then these results will help illustrate
136 that the selection of an appropriate nucleation parameterization cannot simply be based on whether it
137 gives a good agreement with observations and that more rigorous investigations and assessments on
138 its fundamental theory and scientific soundness are needed. The predicted particle number
139 concentrations and size distributions with those nucleation parameterizations are analyzed and
140 evaluated against available measurements in Atlanta where the nucleation involving H_2SO_4 was
141 observed (e.g., McMurry et al., 2000). The controlling atmospheric processes in shaping particle size
142 distributions (e.g., mass, number, and surface area) are studied with a process analysis (PA) tool
143 imbedded in CMAQ and additional sensitivity simulations. While such PA has been conducted in
144 several studies (e.g., Zhang et al., 2005, 2007, 2009b; Yu et al., 2008; Wang et al., 2009; P. Liu et al.,
145 2010a, b; X.-H. Liu et al., 2010a), most focus on the mixing ratios of gases and mass concentrations
146 of PM. To our best knowledge, none of the published PA studies focused on PM number
147 concentrations and surface areas.

148 **2. Model Testbed and Experiment Design**

149 The 3-D modeling domain covers the contiguous U.S. and a small portion of southern Canada
150 and northern Mexico, with a horizontal resolution of 32-km. The vertical resolution is 21 layers from
151 the surface to ~160 mb. The simulation period is June 12-28, 1999. The meteorological fields were
152 generated by the U.S. EPA Atmospheric Modeling and Analysis Division using the Pennsylvania

153 State University (PSU) / National Center for Atmospheric Research (NCAR) Mesoscale Modeling
154 System Generation 5 Version 3.4 (MM5) with four-dimensional data assimilation (FDDA). The
155 EPA's National Emissions Inventories (NEI) 99 version 3 is used to generate a gridded emission
156 inventory for all gas and primary PM species for the contiguous U.S. using the Sparse Matrix
157 Operator Kernel Emissions system (SMOKE1.4). The initial conditions (ICONs) and boundary
158 conditions (BCONs) are set to be those of clear tropospheric air conditions as described in Yu et al.
159 (2004). A spin-up period of two days (June 12-13) is used to minimize the influence of ICONs. All
160 simulations use the Statewide Air Pollution Research Center Mechanism (SAPRC99, Carter, 2000)
161 and the AERO3 aerosol module. The meteorological and chemical predictions from the baseline
162 simulation with KU98 were evaluated using available surface, aircraft, and satellite data by Liu and
163 Zhang (2010a). Both MM5 and CMAQ perform reasonably well for major meteorological variables
164 (i.e., temperature, relative humidity, wind direction, planetary boundary layer height, and
165 precipitation), surface concentrations of chemical species (i.e., O_3, $PM_{2.5}$, sulfate, and ammonium),
166 and vertical profiles of temperature and sulfur dioxide, although small to moderate biases are found
167 for most variables evaluated. This paper focuses on the analysis and evaluation of the simulation
168 results for PM number, volume, surface areas from the CMAQ simulations with the 11 nucleation
169 parameterizations and 5 additional sensitivity simulations for a 15-day period of June 14-28, 1999.
170 Only a small fraction of nucleated particles (i.e., < ~1.5 nm) will survive the competition
171 between the rates of growth and removal processes and grow to the CCN size (~100 nm). The
172 growth mechanisms of nucleated particles to the minimal detectable particle size (~2-4 nm) and to the
173 CCN size remain unknown and may involve many processes such as condensation of nucleating
174 vapor, activation of soluble vapor, heterogeneous nucleation, charged-enhanced condensation,
175 coagulation, multi-phase chemical reactions (Kulmala et al., 2004a), and many species such as
176 H_2SO_4, H_2O, NH_3, aromatic acids, and aminium salt (Eisele and McMurry, 1997; Kulmala et al.,
177 2000; R. Zhang et al., 2004; Smith et al., 2008, 2010). The growth rate of the nucleated particles to

178 particles at 2-4 nm is estimated to be about 2 nm h^{-1} (Eisele and McMurry, 1997), and that of the
179 particles at 2-4 nm to the CCN size is about 1-22 nm h^{-1} (Kulmala et al., 2004b; Kuang et al., 2009) .
180 Such a growth needs to be taken into account when the nucleation parameterizations are used to
181 predict new particle formation rates and their growth into the CCN size in 3-D models. In addition to
182 the uncertainties in the nucleation parameterizations used and aerosol thermodynamic and dynamic
183 processes treated, an additional uncertainty in simulating particle number concentrations lies in
184 whether and how the model treats the growth of particles at different stages before they grow to the
185 simulated smallest size range (i.e., Aitken mode for CMAQ, which is typically considered to contain
186 particles with diameters of 10-100 nm). Recent progress has been made to simulate such a growth
187 using either an empirical growth rate based on measurements (e.g., Kerminen and Kulmala, 2002); or
188 a particle growth module/parameterization (e.g., Pierce and Adams, 2007; Elleman and Covert, 2009
189 b; Kuang et al., 2009), or explicitly simulating the miscrophysics of particles from 1 nm to > 10 μm
190 using a 3-D chemical transport model with a size-resolved aerosol microphysical module (e.g.,
191 Spracklen et al., 2008; Yu and Luo, 2009). CMAQ, however, does not simulate the loss of nucleated
192 particles by collision and the subsequent growth of "survived" particles from 1 nm to Aitken-mode,
193 which will introduce inaccuracies and/or uncertainties in the simulated new particle formation rate
194 and the number concentrations and size distribution of $PM_{2.5}$. By assuming a minimal detectable
195 particle diameter of 2 nm, the new particle formation rates calculated by a nucleation
196 parameterization in CMAQ actually represent their upper limits, because the true new particle
197 formation rates should be always smaller than the nucleation rates. As shown in Zhang et al. (2010b)
198 (the Part I paper), the nucleation rates calculated by some parameterizations may exceed an upper
199 limit prediction of collision-controlled nucleation in terms of dimer production rate and formation
200 rate of particles with 2 nm diameter (McMurry, 1980,1983). If the mass production rate calculated
201 from the number production rate in CMAQ exceeds the H_2SO_4 vapor production rate, it is then
202 capped by the H_2SO_4 vapor production rate and the number production rate is reset to that based on

203 the H_2SO_4 vapor production rate, assuming that the particles are 2 nm in diameter. This cap is
204 equivalent to the maximum new particle formation rate, Max *J*, for particles with 2 nm diameter (i.e.,
205 $J_{2\,nm}$) defined in the Part I paper. The production rate of the newly-formed particles at 2 nm is then
206 used to solve the rate of change in the number concentrations of Aitken mode following the approach
207 of Binkowski and Roselle (2003). The new particle number and mass concentrations in Aitken mode
208 calculated using this method represent an upper limit estimation because CMAQ neglects the loss of
209 some particles as they grow from 2 nm to 10-100 nm.

210 Two sets of model experiments are conducted. The first set consists of a baseline simulation
211 with the default nucleation parameterization of Kulmala et al. (1998) and 10 alternative
212 parameterizations (i.e., Harrington and Kreidenweis (1998), Vehkamäki et al. (2002), Pandis et al.
213 (1994), Fitzgerald et al. (1998), Yu (2008), Napari et al. (2002), Merikanto et al. (2007) with
214 corrections in Merikanto et al. (2009b), Yu (2006), Sihto et al. (2006), and Kuang et al. (2008)). The
215 objectives of this set of experiments are to assess the uncertainties with nucleation parameterizations
216 and their relative accuracies in terms of reproducing particle number and size distributions under an
217 urban environment and to make recommendations regarding the appropriateness of their applications
218 under polluted environments. The particle number concentrations and size distributions predicted
219 with different nucleation parameterizations are compared with available observations in the
220 southeastern U.S. Several special field studies were carried out in Atlanta, GA to study atmospheric
221 particle formation, evolution, and health effects. These include the Aerosol Research Inhalation
222 Epidemiological Study (ARIES) (Van Loy et al., 2000; Woo et al., 2000) during 1998-2000 and the
223 Aerosol Nucleation and Real Time Characterization Experiment (ANARChE) study of nucleation in
224 August 2002 (McMurry et al., 2005). These measurements were carried out at the Jefferson Street
225 (JST) site, located about 4 km northwest of downtown Atlanta (Woo, 2003). Size distributions in the
226 3 nm to 2 μm range were measured and subsequently segregated into three size ranges (i.e., geometric
227 mean diameter < 10 nm, 10-100 nm, and 0.1-2 μm). High concentrations (up to 2.7×10^5 number

228 cm^{-3}) of freshly-nucleated 3-10 nm particles have been frequently observed in summer in Atlanta, GA
229 (McMurry et al., 2000; Woo et al., 2001). The enhancement of ultrafine particle concentrations often
230 occurred near noontime and was associated with high solar radiation. It was suggested that these
231 nanoparticles were formed through a photochemically-driven collision-controlled nucleation process
232 involving H_2SO_4 (McMurry et al., 2000). While the derived nucleation rates based on observed
233 particle size distributions and H_2SO_4 vapor concentrations from ANARChE are used in the Part I
234 paper to evaluate simulated nucleation rates from various parameterizations without considering other
235 atmospheric processes, the observed number, surface, and volume concentrations of PM with
236 diameter less than 2 μm (PM_2) from ARIES during the period of June 14-28, 1999 at JST, Atlanta,
237 GA are used to evaluate CMAQ predictions in this Part II paper (note that no derived nucleation rates
238 are available from the ARIES particle size observations). The comparison is conducted between
239 simulated Aitken-mode PM without cut-off in size and observed $PM_{0.1}$ with an upper cut-off diameter
240 of 0.1 μm, between simulated Accumulation-mode PM without cut-off in size and observed $PM_{0.1\text{-}2}$
241 with a diameter range of 0.1-2 μm, and between a number of size-resolved bins in the diameter size
242 range with lower and upper cut-off geometric mean diameters of 0.00306 μm and 2 μm, respectively
243 for simulated and observed PM_2,. The first two comparisons represent an approximation because the
244 tails of the log-normal size distributions for Aitken- and Accumulation-mode PM extend beyond the
245 cut-off diameters bounded for observed $PM_{0.1}$ and $PM_{0.1\text{-}2}$, whereas the last comparison provides the
246 most rigorous size-resolved evaluation.

247 The second set consists of a simulation with process analysis and five simulations to study the
248 sensitivity of model PM number predictions to several model parameters or processes of interest.
249 The objectives of this set of experiments are to identify the most important processes in controlling
250 particle properties and to estimate uncertainties associated with assumed model parameters/processes
251 that will affect PM number and size predictions for potential model improvements. Important
252 atmospheric processes in determining particle mass, number, and surface area are first identified with

253 the Integrated Process Rate (IPR) of the PA tool for locations representative of remote, rural, and
254 urban conditions. Sensitivity simulations are then conducted to further investigate the model
255 treatments for several atmospheric processes such as emissions and dry deposition and related
256 parameters such as initial PM size distribution, the fractions of Aitken-mode PM in total PM
257 emissions, and dry deposition velocity.

258 **3. Comparisons of Model Predictions with Various Nucleation Parameterizations**

259 **3.1 Spatial Distribution of Predicted PM Number, Volume, and Surface Area**

260 Figure 1 shows 15-day mean spatial distributions of hourly $PM_{2.5}$ number concentrations from
261 the simulations with the 11 nucleation parameterizations and maximum nucleation rate. The
262 simulation with $J_{2\ nm}$ gives $PM_{2.5}$ number concentrations of 10^4 - 2.7×10^6 cm^{-3} over land and 10^3 -
263 10^4 cm^{-3} over oceanic areas. Those over land are $10^2 - 7.5 \times 10^4$ cm^{-3} for PA94, $10^2 - 2 \times 10^4$ cm^{-3}
264 for FI98, $10^3 - 1.4 \times 10^5$ cm^{-3} for HK98, $10^2 - 4.9 \times 10^3$ cm^{-3} for KU98, $10^2 - 5.2 \times 10^3$ cm^{-3} for
265 VE02, $10^2 - 4.8 \times 10^3$ cm^{-3} for YU08, $10^4 - 1.4 \times 10^6$ cm^{-3} for NA02, $10^2 - 4.8 \times 10^3$ cm^{-3} for ME07,
266 $10^2 - 5.0 \times 10^3$ cm^{-3} for YU06, $10^4 - 1.8 \times 10^5$ cm^{-3} for SI06, and $10^3 - 2.3 \times 10^5$ cm^{-3} for KU08. The
267 large differences among the predicted PM number concentrations are due to differences in theoretical
268 bases, mathematical equations, processes and assumptions considered in various parameterizations to
269 calculate nucleation rates, as described in the Part I paper. Those over oceanic areas simulated by
270 various parameterizations are typically in the range of $10^2 - 10^3$ cm^{-3}. According to the magnitude of
271 the predicted PM number concentrations, the 11 parameterizations can be grouped into four distinct
272 subgroups with values on the order of 10^6 cm^{-3} (i.e., NA02), 10^5 cm^{-3} (i.e., SI06, KU08, and HK98),
273 10^4 cm^{-3} (i.e., PA94 and FI98), and 10^3 cm^{-3} (i.e., KU98, VE02, YU08, ME07, and YU06) over
274 CONUS. The magnitudes and spatial distributions of volume concentrations simulated by all
275 parameterizations are very similar, ranging from 0.1-14.5 μm^3 cm^{-3} (Figures not shown). The surface
276 concentrations simulated by all parameterizations have spatial distributions similar to those of
277 number concentrations (Figures not shown); and their values are proportional to number

278 concentrations and PM mean diameters, ranging from 3.2 to 379 μm^2 cm^{-3} for NA02, 3.1-350 μm^2
279 cm^{-3} for SI06, KU08, and HK98, 2.9 - 327 μm^2 cm^{-3} for PA94 and FI98, and 2.8 – 290 μm^2 cm^{-3} for
280 KU98, VE02, YU08, ME07, and YU06.

281 **3.2 Temporal Variation of Predicted PM Number, Volume, and Surface Area**

282 Figure 2 shows the predicted number concentrations of Aitken-mode particles at JST, Atlanta,
283 GA and Great Smoky Mountains (GRSM), TN. The number concentrations of observed $PM_{0.1}$ at JST
284 are plotted for an approximate comparison (no observational data are available at GRSM). Note that
285 a logarithmic scale is used to best show the simulated particle number concentrations that vary by
286 several orders of magnitude (10^2 to 10^6 cm^{-3}). Such a log scale somewhat smoothes out the temporal
287 variations of observed particle number concentrations that vary from $> 10^2$ to $< 10^5$ cm^{-3} throughout
288 the simulation period but only change within 1 order of magnitude during nucleation events (e.g.,
289 from 2.5×10^4 to 1.0×10^5 cm^{-3} on June 24, 1999). At JST, the predicted number concentrations for
290 Aitken-mode PM range from 396 to 22661 cm^{-3} by PA94, 432 to 10765 cm^{-3} by FI98, 523 to 243850
291 cm^{-3} by HK98, 285 to 6010 cm^{-3} by KU98; 297 to 6545 cm^{-3} by VE02, 239 to 2610 cm^{-3} by YU08,
292 580 to 1674600 cm^{-3} by NA02, 231 to 1169 cm^{-3} by ME07, 269 to 3179 cm^{-3} by YU06, 2284 to
293 134090 cm^{-3} by SI06, and 656 to 130240 cm^{-3} by KU08. For comparison, the observed number
294 concentrations for Aitken-mode PM at JST range from 2039 to 102309 cm^{-3}. Compared with the
295 observed values, the predicted Aitken-mode PM number concentrations are consistently lower by up
296 to a factor of 96 for PA94, 95 for FI98, 287 for KU98, 276 for VE02, 337 for ME07, 290 for YU06,
297 and 320 for YU08; either higher by up to a factor of 30, 204, 41, and 29 or lower by up to a factor of
298 81, 97, 25, and 69 for HK98, NA02, SI06, and KU08, respectively. The PM number concentrations
299 from all parameterizations except for NA02 are well below those by the simulation with $J_{2\ nm}$,
300 whereas those from NA02 sometime reach or are close to the upper limits. Among all 11
301 parameterizations tested, the peak number concentrations predicted by the power law of SI06 give the
302 closest agreement to the observed values at JST; the ternary parameterization of NA02, the binary

303 parameterization of HK98, and the power law of KU08 also perform better than other
304 parameterizations in terms of simulated number concentrations. NA02 gives a good agreement in this
305 study and other studies, however, for a wrong reason since it has several fundamental
306 problems/technical flawed treatment as indicated previously and also described in more details in
307 Zhang et al. (2010b), which have been corrected in ME07. The Aikten-mode number concentrations
308 given by ME07 are lower by factors of 1-4246 than those from NA02, which, however, does not
309 reproduce the observed particle number concentrations for the urban environment, due likely to the
310 fact that other nucleation mechanisms may dominate in Atlanta. None of the 11 parameterizations
311 reproduce the temporal variations of the observed $PM_{0.1}$ number concentrations at JST. The
312 simulated PM number concentrations from all parameterizations show a very strong diurnal variation.
313 The peak values occur at noontime when the solar radiation is the strongest and the number
314 concentrations of H_2SO_4 are the maximum, and the values during daytime and nighttime vary by
315 several orders of magnitude. By contrast, the observed values can peak at certain times of a day
316 including both daytime and nighttime (e.g., 1 a.m. on June 16 and 23) and remained high for 2 or
317 more days, the differences between daytime and nighttime values are typically within a factor of 2.
318 The lack of diurnal variations in observed number concentrations indicate that some new particles
319 produced during daytime may remain at night due likely relatively slow removal processes, which are
320 not captured well by CMAQ.

321 Five parameterizations (i.e., ME07, YU08, YU06, KU98, and VE02) give the lowest number
322 concentrations that differ from the highest number concentrations predicted by SI06 by up to factors
323 of 535 and 496 at GRSM and JST, respectively. The variations in the predicted number
324 concentrations among all parameterizations tested are associated with several factors including the
325 number concentration of H_2SO_4 produced (N_{H2SO4}) via the gas-phase oxidation of SO_2 by OH radicals
326 for all nucleation parameterizations, temperature (T), and relative humidity (RH) for binary and
327 ternary nucleation parameterizations (except for PA94 in which temperature-dependence of

328 nucleation rates is not accounted for and HK98 in which the T- and RH-dependence of nucleation
329 rates are rather weak), and the ambient concentrations of NH_3 (C_{NH3}) for ternary nucleation
330 parameterizations. With a correct kinetic treatment for hydrate formation, VE02 gives nucleation
331 rates slightly higher than those by KU98 (by up to a factor of 2.4 at JST and 2.8 at GRSM) during
332 most time periods. This increase is due mainly to a stronger N_{H2SO4}-dependence in VE02 (see Figure
333 1 in the Part I paper). In the parameterization of Vehkamäki et al. (2002), the nucleation rate is given
334 by an exponential of first- to third-order polynomial of Ln (N_{H2SO4}), whereas that in Kulmala et al.
335 (1998) is given by an exponential of first-order polynomial of Ln (N_{H2SO4}). In Yu (2008), the BHN
336 of H_2SO_4 and H_2O is treated as quasi-unary nucleation (QUN) process for H_2SO_4 in equilibrium with
337 H_2O and an analytical expression was derived based on a kinetic collision theory to calculate the
338 H_2SO_4–H_2O QUN rate as a function of N_{H2SO4}, T, and RH. In Yu (2006), the ternary nucleation rates
339 for a system involving H_2SO_4, NH_3, and H_2O are calculated using a kinetic THN model with the NH_3
340 enhancement effect constrained by laboratory experimental results. Yu (2008) showed that the QUN
341 rates are lower than those of VE02 that are based on the classical BHN theory; this trend is consistent
342 with the results shown in Figures 1 and 2. Yu (2006) reported a negligible contribution of THN rates
343 to new particle formation in the boundary layer, which is also consistent with comparison between
344 observations and simulated values from YU06 in Figure 2. As shown in Figures 1 and 2, NA02 that
345 is based on the classical THN theory gives much higher nucleation rates (up to 3 orders of magnitude
346 at JST) than YU06 due to a much higher enhancement in the presence of ppt level of NH_3, whereas
347 the laboratory measurements show only one to two orders of magnitude enhancement in the presence
348 of several ppt to several ppm level of NH_3 (Yu, 2006). YU06 gives much lower THN rates than
349 NA02 because it uses laboratory data to constrain the rates calculated from the classical THN theory.
350 The predicted N_{H2SO4} and C_{NH3} are much higher at JST than at GRSM, resulting in much larger
351 amplitudes of the predicted number concentrations among various parameterizations at JST than at
352 GRSM. The PM number concentrations from all parameterizations are well below those by the

353 simulation with J_{2nm} at GRSM. Although no observed PM number concentrations were available for
354 the current model evaluation, some studies have shown that organics may play an important role in
355 the observed nucleation events in the forested region such as GRSM (Kulmala et al., 1998; Kavouras
356 et al., 1998; O'Halloran et al., 2009) due to the availability of high biogenic volatile organic
357 compound (VOC) emissions and resultant concentrations (Day et al., 1997; Blando et al., 1998).
358 Figure 3 shows the number concentrations of accumulation-mode particles predicted with 11
359 nucleation parameterizations at JST and GRSM. The number concentrations of observed $PM_{0.1-2}$ at
360 JST are plotted for an approximate comparison. Compared with predicted Aitken-mode PM number,
361 the predicted accumulation-mode PM number concentrations at JST are in much better agreement
362 with the observations despite some overpredictions during most time periods. The predicted number
363 concentrations for accumulation-mode PM range from 269 to 6694 cm^{-3} by PA94, 267 to 6683 cm^{-3}
364 by FI98, 281 to 8665 cm^{-3} by HK98, 266 to 6680 cm^{-3} by KU98, VE02, YU06, YU08, and ME07,
365 274 to 8013 cm^{-3} by NA02, 271 to 7053 cm^{-3} by SI06, and 269 to 7046 cm^{-3} by KU08. For
366 comparison, the observed number concentrations for accumulation-mode PM at JST range from 254
367 to 7750 cm^{-3}. Similar to the Aitken-mode predictions, five parameterizations (i.e., KU98, VE02,
368 YU06, YU08, and ME07) give the lowest number concentrations, four parameterizations (i.e., HK98,
369 NA02, SI06, and KU08) give the highest predictions, with a difference by up to factors of 3.2 and 5.4
370 at GRSM and JST, respectively. The predictions from NA02 sometimes reach or are close to the
371 upper limit of simulated accumulation-mode PM number concentrations using $J_{2\ nm}$ at both JST and
372 GRSM, the rest of parameterizations are below those limits. The very low number concentrations (<
373 100 cm^{-3}) on June 15, 25, and 27 at GRSM are caused by extremely low H_2SO_4 vapor concentrations
374 during a few midnight to early morning hours (e.g., 2-4 a.m. on June 15, 1-4 a.m. on June 25, 0-1
375 a.m. on June 27), mid-afternoon hours (e.g., 2-5 p.m. on June 24), or morning hours (e.g., 7-11 a.m.
376 on June 27), as a result of heavy precipitation. Such rain events influence the PM number

377 concentrations simulated by all parameterizations because of their strong dependence on H_2SO_4 vapor
378 concentrations.

379 Figures 4 and 5 show the observed and predicted volume concentrations and surface area,
380 respectively, for both PM modes at JST. All parameterizations significantly underpredict the volume
381 concentrations for Aitken-mode on June 14-16 and June 26-28 but significantly overpredict those on
382 June 17-20. All parameterizations significantly underpredict the surface areas for Aitken-mode
383 during most days except June 17-20 and June 25. The simulation with $J_{2\ nm}$ gives much higher
384 surface areas than all nucleation parameterizations for most daytime hours on June 17-20, 21-24, and
385 25. During the period of 1:00 p.m. June 17 to 8:00 p.m. June 20, the predicted H_2SO_4 vapor
386 concentrations are the highest (5.0×10^5 to 2.8×10^8 molecules cm^{-3}, with an average of 7.0×10^7
387 molecules cm^{-3}), the predicted *RH* values are the lowest (33.2-77.5%, with an average of 54.5%), and
388 the predicted temperatures are in the range of 288-300 K with an average of 294 K. Under these
389 conditions, the new particle formation rates predicted from all parameterizations increase with
390 increasing H_2SO_4 vapor concentrations; increase with increasing *RH* except for NA02; and decrease
391 with increasing *T* (except for PA94, SI06, and KU08 that do not depend on *T*). The H_2SO_4-
392 dependence dominates, resulting in a significant increase of Aitken-mode PM mass concentration,
393 thus high volume concentrations and surface areas of Aitken-mode PM. The overpredictions in the
394 volume concentrations and surface areas of Aitken-mode PM are therefore likely due to the
395 participation of excessive amounts of H_2SO_4 vapor concentrations in nucleation (rather than
396 condensation) during this time period. The volume concentrations and surface areas for
397 accumulation-mode are significantly underpredicted on June 14-19 and June 21-24. An evaluation
398 of predicted 24-hr average sulfate concentrations against the observations from SOS99 showed a
399 significant overprediction (by a factor of 2-3) on June 19-25 and a slight underprediction (by 5-7%)
400 on June 14-17 (P. Liu et al., 2010a). The simulated cloud fraction and liquid water content were low
401 during June 19-25, indicating that the photochemical oxidation of SO_2 rather than aqueous-phase

402 oxidation of SO_2 dominates the formation of H_2SO_4 thus sulfate. The overprediction in sulfate during
403 this time period thus indicates a sufficient amount of H_2SO_4 for nucleation (Neither observed
404 temperatures and RHs nor hourly H_2SO_4 or sulfate concentrations are available for model evaluation
405 during this time period). The underpredictions in volume and surface area concentrations for
406 accumulation-mode PM are indeed caused by underpredictions in other PM species such as organic
407 and black carbon (P. Liu et al., 2010a). In addition to uncertainties in predicted meteorology (e.g.,
408 higher simulated wind speeds and PBL height than observations as shown in P. Liu et al., 2010a),
409 several factors may contribute to such underpredictions. For example, these may include the
410 uncertainties in the emissions of black carbon, primary organic carbon, and precursors of secondary
411 organic aerosols, insufficient condensational growth of PM, uncertainty in the assumed initial size
412 distribution, as well as the use of a 32-km horizontal grid resolution that is too coarse to resolve the
413 local emission strengths and distributions needed to reproduce point-wise observations (Zhang et al.,
414 2006; P. Liu et al., 2010a).

415 For Aitken-mode PM predictions, the simulation with $J_{2\ nm}$ predicts the highest number
416 concentrations and surface areas but the lowest volume concentrations because it predicts the smallest
417 number and volume mean diameters among all nucleation parameterizations tested. When sufficient
418 H_2SO_4 vapor is available for nucleation (e.g., June 17-21), ME07 and YU06 give the highest and the
419 second highest number mean diameters, and the highest and the 2nd highest volume mean diameters,
420 resulting in the 5th highest and the 4th highest volume concentrations despite their relative low number
421 concentrations and surface areas. KU98 and VE02 also give high number and volume mean
422 diameters (the 3rd and 4th, respectively, resulting in the 1st and 3rd highest volume concentrations).
423 YU08 gives the second highest volume concentrations. The overpredictions in volume
424 concentrations and surface areas by PA94 and FI98 are similar; they are larger than those from HK98,
425 NA02, KU08, and SI06 over most time periods. For accumulation-mode PM, the differences are
426 much smaller in the simulated surface areas and negligible in the simulated volume concentrations

predicted by the 11 nucleation parameterizations. None of them reproduce well the temporal variations of volume concentrations and surface areas for both modes during most of time.

3.3 PM Size Distributions

The observed PM_2 number size distributions in Atlanta exhibit three distinct modes, most peaks in the size ranges of 0.00306-0.00406 μm, 0.01863-0.03694 μm, and 0.0499-0.0786 μm (with an exception that the third mode peaks in the range of 0.147-0.242 μm on June 18, 20, and 26). The observed volume distributions exhibit one to three distinct modes, having one mode on June 15, 23, 24, 27, and two modes on June 14, 16-22, and 25-27 and three modes on June 27 and 28. The observed surface area distributions exhibit one to two distinct modes, having one mode on June 17-21 and 25 and two modes on June 14-16, 22-24, 26, and 28. Figure 6 shows the observed vs. predicted 24-hr average number, volume, and surface area size distributions on three representative days: June 18, 20, and 23 among the 15-day period. On all three days, KU98, VE02, ME07, YU06, and YU08 reproduce relatively well the number concentrations for the 3rd mode (i.e., the accumulation mode) but significantly underpredict those for the 1st and 2nd modes (i.e., the nucleation and Aitken modes). PA94 and FI98 also fail to reproduce the 1st mode, but they give slightly better predictions for the 2nd mode than the above five parameterizations. For comparison, HK98, SI06, and KU08 reproduce the number concentrations of the 1st mode to some degrees on all days despite overpredictions (e.g., June 18) or underpredictions (e.g., June 23) on some days; they also sometimes underpredict those for the 3rd mode (e.g., on June 18). NA02 captures well the 2nd mode but also sometimes underpredicts the number concentrations of the 3rd mode (e.g., June 18), it captures the 1st mode on most days but fails on June 17, 23, and 25. While all simulations generally reproduce the observed Aitken and accumulation modes whose distributions appear lognormal, the observed size distribution of the nucleation mode is generally poorly characterized because the use of a log-normal distribution in CMAQ cannot well resolve the observed non-lognormal distribution of nanoparticles that are freshly nucleated (typically with a diameter < 5 nm) as reported by McMurry et al. (2000) and McMurry and

Woo (2002). In addition, the assumption that Aitken-mode particles are produced at the same rate as that of newly-formed particles at 2 nm sometimes leads to artificial increases in the number concentrations in the Aitken mode (e.g., June 18 and 20) and underpredicts those in the nucleation mode (e.g., June 18, 20, and 23). Considering the loss of nucleated particles by collision and the subsequent growth of "survived" particles from 1 nm to Aitken-mode can give more realistic size distributions, as shown in Elleman et al. (2009b). All parameterizations exhibit a similar underprediction for the volume concentrations and surface areas except on June 20-21 and 26-27, with the largest mean diameter predicted by ME07 and YU06, and the smallest mean diameter predicted by SI06. These results are quite consistent with the predicted hourly number, volume, and surface areas shown previously.

3.4 Statistical Evaluation

The hourly total number, volume, and surface areas during June 14-28 predicted for $PM_{2.5}$ (i.e., the sum of Aitken and accumulation mode PM) are compared with the observed values for PM_2 using various statistical metrics, as shown in Tables 1(a) to 1(c), respectively. The simulation with J_{2nm} significantly overpredicts (by a factor of 13.5) the total number concentrations. Seven parameterizations significantly underpredict them (by factors of 14.5, 14.1, 13.7, 13.2, 12.4, 9.2, 7.6, and 1.6 for ME07, YU06, YU08, KU98, VE02, FI98, and PA94, respectively). The remaining four parameterizations also underpredict the total number concentrations but to a much smaller extent (by factors of 2.5, 2.0, 1.6, and 1.5 for KU08, HK98, NA02, and SI06, respectively). While the number concentrations for accumulation-mode PM are overpredicted by factors of 1.4 to 2.2 for all parameterizations, those for Aitken-mode PM are significantly underpredicted by factors of 1.7 to 47 for all parameterizations except for NA02 and SI06, resulting in an overall underprediction in the number concentrations of $PM_{2.5}$. The total volume concentrations for $PM_{2.5}$ are underpredicted by factors of ~1.7 by all the parameterizations, largely because the underprediction (by factors of 1.4 to 1.8) in the volume concentrations of accumulation-mode PM overwhelms the overprediction (by

477 factors of 1.2 to 1.6) in the volume concentrations of Aitken-mode PM by all parameterizations
478 except for KU08, SI06, NA02, and HK98 (which underpredict the volume concentrations of both
479 Aitken- and accumulation-mode PM by factors of 1.2-1.4 and 1.7-1.8, respectively). The total
480 surface areas are underpredicted by factors of ~1.9 for KU98, VE02, YU08, ME07, YU06, 1.7 for
481 FI98, and PA94, 1.6 for HK98, NA02, KU08, and SI06, and 1.2 for the simulation with $J_{2\ nm}$, largely
482 due to the underpredictions in the surface areas of both Aitken- and accumulation-mode PM (by
483 factors of 1.4 to 3.2 and 1.5 to 1.9, respectively) by all nucleation parameterizations. Among the 11
484 parameterizations, the top four parameterizations having the closest agreement to observations are
485 SI06, NA02, HK98, and KU08 for the total number concentrations, and SI06, NA02, KU08, and
486 HK98 for the total surface area concentrations. The performance of all parameterizations in terms of
487 the total volume concentrations is very similar. Overall, SI06 gives the best statistical performance
488 among all parameterizations tested.

489 A more rigorous evaluation is conducted for the predicted 24-hr average number, volume, and
490 surface area size distributions with the 11 nucleation parameterizations by integrating their lognormal
491 size distributions for 39 segregated size sections over the diameter range of 0.001 to 2 μm and then
492 comparing against the ARIES measurements in the diameter range of 0.00306 to 2 μm for PM_2. The
493 upper bound of the observed segregated size sections are 0.00306, 0.00406, 0.0049, 0.00592,
494 0.00716, 0.00787, 0.00866, 0.00952, 0.01048, 0.01153, 0.01268, 0.01396, 0.01537, 0.01692,
495 0.01863, 0.02052, 0.02261, 0.02493, 0.02748, 0.03032, 0.03346, 0.03694, 0.04081, 0.0451, 0.0499,
496 0.056, 0.0609, 0.0663, 0.0722, 0.0786, 0.102, 0.147, 0.242, 0.34, 0.54, 0.71, 1.04, 1.23, and 2.0 μm.
497 Tables 2(a)-2(c) show the size-resolved statistics for number, volume, and surface area size
498 distributions over the 15-day period. While the simulation with $J_{2\ nm}$ overpredicts size-resolved
499 number concentration by a factor of 12.2, other parameterizations underpredict it by factors of 1.3 to
500 12.4. The size-resolved volume concentrations are underpredicted by factors of 1.8-2.0. The size-
501 resolved surface areas are underpredicted by factors of 2.1 for ME07, KU98, and VE02, 2.0 for YU08

and YU06, 1.8 for FI98 and PA94, 1.6 for HK98, NA02, and SI06, 1.3 for KU08 and the simulation with $J_{2\ nm}$. Among the 11 parameterizations, the top four parameterizations having the closest agreement to observations are NA02, SI06, HK98, and KU08 for the size-resolved number concentrations, SI06, KU08, HK98, and NA02 (note that YU06 and YU08 also rank the 4th) for the size-resolved volume concentrations, and KU08, SI06, NA02, and HK98 for the size-resolved surface area concentrations. Overall, SI06 gives the best performance for all three size-resolved variables evaluated. These results are quite consistent with the statistics obtained with the total number and surface areas shown in Tables 1(a) and 1(c). The evaluation of size-resolved volume concentrations can discern the performance of various parameterizations better than the evaluation of the total volume concentrations which gives nearly identical performance for all parameterizations.

4. Process and Sensitivity Studies for Controlling Processes

4.1 Process Analysis

Process analysis embedded in CMAQ includes two components: the integrated process rate (IPR) and the integrated reaction rate (IRR). The IPR analysis is conducted to quantify the relative contributions of major atmospheric processes to PM mass, number, and surface areas. Table 3 summarizes the 15-day average hourly changes in PM number, mass, and surface areas concentrations of Aitken- and accumulation-mode PM (referred to as PM-AIT and PM-ACC, respectively) in the planetary boundary layer (PBL) (i.e., model layers 1-14, corresponding to 0 to ~2.5 km) due to seven major atmospheric processes at JST, Atlanta, GA, Los Angeles (LAX), CA, and GRSM, TN. The seven major atmospheric processes include horizontal transport, vertical transport, emissions, dry deposition, PM processes, cloud processes, and mass balance adjustment. PM processes represent the net effect of PM thermodynamics, new particle formation due to homogeneous nucleation, gas-to-particle mass transfer, condensation of H_2SO_4 and organic compounds on preexisting particles, and coagulation in and between Aitken and accumulation modes. Cloud processes represent the net effect of cloud attenuation of photolytic rates, convective and non-

527 convective mixing and scavenging by clouds, aqueous-phase chemistry, and wet deposition. The
528 mass balance adjustment corrects the species mass inconsistency and imbalance caused by highly-
529 parameterized physical and cloud algorithms such as advection scheme.

530 At JST, the production of PM-AIT number is dominated by PM processes (2.6×10^3 cm^{-3} hr^{-1}
531 or by 97.2%), and its loss is dominated by dry deposition (-1.4×10^3 cm^{-3} hr^{-1} or -51.6%) and cloud
532 process (-1.1×10^3 cm^{-3} hr^{-1} or -39.8%). Although intra- and inter-mode coagulation plays an
533 important role to its loss, the production of new particles through homogeneous nucleation is greater
534 than this loss, resulting in a net production due to PM processes. The controlling processes for PM-
535 ACC number are quite different, with primary emissions as the only production process (1.0×10^2
536 cm^{-3} hr^{-1} or 100%) and horizontal transport and cloud processes (-62 cm^{-3} hr^{-1} or -58.3% and -30 cm^{-3}
537 hr^{-1} or -28.3%, respectively) dominating its loss. The contributions of PM processes and dry
538 deposition to its loss are relatively small (-6.6% and -3.4%, respectively). The loss processes such as
539 coagulation within PM-ACC and between PM-AIT and PM-ACC dominate over the gain processes
540 such as the growth of PM-AIT via gas-to-particle conversion and self-coagulation of PM-AIT to form
541 PM-ACC, leading to a small net loss due to PM processes. At LAX, PM processes also dominate the
542 production of PM-AIT number concentrations (8.4×10^4 cm^{-3} hr^{-1} or 99.1%), and dry deposition and
543 horizontal transport dominate its loss (-4.8×10^4 cm^{-3} hr^{-1} or -54.8% and -3.9×10^4 cm^{-3} hr^{-1} or -
544 44.8%, respectively), reflecting the influences of dry weather conditions and sea-breezes. For PM-
545 ACC number, emissions, PM processes, and vertical transport contribute to its production at rates of
546 70, 32, and 14 cm^{-3} hr^{-1} (or 60.7%, 27.5%, and 11.8%), respectively, and horizontal transport and dry
547 deposition contribute to its loss at rates of -110 (or -91.8%) and 8 cm^{-3} hr^{-1} (or -6.8%), respectively.
548 The dominant processes are quite different at GRSM, a remote mountain site that is affected by long
549 range transport of air pollutants from upwind urban locations. The production of PM-AIT number is
550 controlled by vertical transport, horizontal transport, and cloud processes with rates of 6.3×10^2, 3.3

551 $\times 10^2$, and 1.3×10^2 cm^{-3} hr^{-1} (or 57.3%, 30.7%, and 11.7%), respectively. Its loss is controlled by
552 PM processes (-1.0×10^3 cm^{-3} hr^{-1} or -91.7%) and dry deposition (-93 cm^{-3} hr^{-1} or -8.3%). At this
553 site, coagulation (rather than homogeneous nucleation) dominates because of lack of sources of
554 H_2SO_4 for nucleation, resulting in a net loss due to PM processes. Vertical transport also contributes
555 predominantly (23 cm^{-3} hr^{-1} or 86.3%) to the production of PM-ACC number. Processes contributing
556 to its loss include cloud processes (-12 cm^{-3} hr^{-1} or -44.5%), horizontal transport (-7.3 cm^{-3} hr^{-1} or -
557 26.4%), PM processes (-6.0 cm^{-3} hr^{-1} or -21.6%), and dry deposition (-2.1 cm^{-3} hr^{-1} or -7.5%).

558 While PM processes (e.g., homogeneous nucleation) provide a dominant source for PM-AIT
559 mass concentration at JST (1.0×10^{-4} $\mu g\ m^{-3}$ hr^{-1} or 98.8%), both PM processes (1.2×10^{-5} $\mu g\ m^{-3}$ hr^{-1}
560 or 49.4%) and vertical transport (1.1×10^{-5} $\mu g\ m^{-3}$ hr^{-1} or 44.6%) are important sources of PM-AIT at
561 LAX. While horizontal transport dominates its loss at LAX (-2.4×10^{-5} $\mu g\ m^{-3}$ hr^{-1} or -94.6%),
562 several processes including horizontal transport, cloud processes, and vertical transport provide
563 important sinks at JST (-4.6×10^{-5}, -3.9×10^{-5}, and -1.1×10^{-5} $\mu g\ m^{-3}$ hr^{-1} or -44%, -36.7%, and -
564 10.9%, respectively). For PM-ACC mass concentration at urban locations, emissions and PM
565 processes dominate their production at rates of 3.5×10^{-3} and 1.9×10^{-3} $\mu g\ m^{-3}$ hr^{-1} (or 64.8% and
566 35.2%) at JST and 2.4×10^{-3} and 7.9×10^{-4} $\mu g\ m^{-3}$ hr^{-1} (or 66.1% and 22.1%) at LAX, respectively.
567 Horizontal transport dominates its loss (-4.5×10^{-3} $\mu g\ m^{-3}$ hr^{-1} or -83.6% at JST and -3.5×10^{-3} $\mu g\ m^{-3}$
568 hr^{-1} or -94.6% at LAX). Compared with LAX, particles at JST have a larger production rate for mass
569 concentrations but smaller number production rates of PM-AIT and PM-ACC. This indicates that
570 particles at JST are larger in size than those at LAX, which is caused by the abundance of sulfate at
571 JST that exists mostly in PM-ACC (0.1-2.5 μm) at JST and that of EC and OM that exist mostly in
572 submicron size range (< ~1 μm) at LAX. Dominant processes for PM-AIT and PM-ACC mass
573 concentrations at GRSM are similar to those for PM-AIT at LAX except for a much higher loss rate
574 due to cloud processes (e.g., -6.2×10^{-5} $\mu g\ m^{-3}$ hr^{-1} or -36.3% at GRSM vs. -7.8×10^{-8} $\mu g\ m^{-3}$ hr^{-1} or -

575 0.3% at LAX for PM-AIT), due to stronger cloud scavenging at GRSM than at LAX. This leads to a
576 lower percentage contribution of horizontal transport to the total loss rate at GRSM (-59.8%) than at
577 LAX (-94.6%) for PM-AIT. The large differences in controlling processes of PM-ACC mass
578 concentrations at urban and rural locations attest a need to develop region-specific (rather than cross-
579 broad) emission control strategies, with a focus on primary PM emissions from local sources in urban
580 areas and those from upwind sources in rural areas. Controlling the emissions of precursors of
581 secondary PM in both rural and urban areas will also be effective. Reduction in primary PM
582 emissions can lead to reduction in secondary PM through reducing the total surface areas available
583 for the heteorogeneous reactions to produce sulfate and nitrate or the secondary organic matter
584 formation through reducing the mass concentrations of absorbing primary organic matter that affects
585 the gas/particle partitioning of semi-volatile organic compounds. Such emission control strategies
586 should also account for the transport of the PM emissions away from the urban regions under
587 prevailing weather conditions.

588 Dominant processes for the surface area concentration of PM-AIT and PM-ACC are generally
589 similar to those for their number concentrations at JST and LAX. At GRSM, dominant processes for
590 the surface area concentration of PM-AIT are different from those for its number and mass
591 concentrations and those for PM-ACC are different from the dominant processes for its number
592 concentration but similar to those for its mass concentrations. At GRSM, vertical and horizontal
593 transport dominate the production of PM-AIT surface area concentration (2.9×10^{-1} μm^2 cm^{-3} hr^{-1} or
594 68.7% and 7.0×10^{-2} μm^2 cm^{-3} hr^{-1} or 16.5%, respectively), and cloud processes and dry deposition
595 dominate their loss with rates of -3.6×10^{-1} and -7.8×10^{-2} μm^2 cm^{-3} hr^{-1} (or -82.3% and -17.7%),
596 respectively. Vertical transport and PM processes dominate the production of PM-ACC surface area
597 at rates of 1.2 and 0.39 μm^2 cm^{-3} hr^{-1} (or 66.3% and 22%), respectively, and horizontal transport and
598 cloud processes dominate its loss at rates of -1.0 and -0.7 μm^2 cm^{-3} hr^{-1} (or -57.1% and -38.8%),
599 respectively, which are similar to the dominant processes for PM-ACC mass concentrations.

600 Figure 7 shows the 15-day average percentage contributions of each process to number, mass,
601 and surface area of $PM_{2.5}$ (i.e., the sum of PM-AIT and PM-ACC) in the PBL at two urban (JST and
602 LAX), two rural (Yorkville (YRK), GA and Penn State (PSU), PA), and two remote locations
603 (GRSM and Olympic National Park (OLY)). At all sites, controlling processes for $PM_{2.5}$ number
604 concentrations are similar to those for PM-AIT, and those for $PM_{2.5}$ mass concentrations are similar
605 to those for PM-ACC (figures not shown), reflecting the dominance of $PM_{2.5}$ number in PM-AIT and
606 $PM_{2.5}$ mass in PM-ACC. Controlling processes for $PM_{2.5}$ surface areas are dominated by those for
607 PM-ACC at JST and LAX because of its dominance in total $PM_{2.5}$ surface areas and by those for both
608 PM-AIT and PM-ACC at GRSM because of their comparable contributions to total $PM_{2.5}$ surface
609 areas. For the production of $PM_{2.5}$ number concentrations, PM processes is the top contributor due to
610 the dominance of homogeneous nucleation over other PM processes (except at GRSM where vertical
611 transport dominates and PM processes play an opposite role (i.e., lead to a net loss); and horizontal
612 transport may be the second most important process at some rural or remote sites (e.g., OLY and
613 GRSM). For the loss of $PM_{2.5}$ number concentrations, dry deposition is the top contributor at all sites
614 except for GRSM where PM processes dominate, and other processes can sometime be the second
615 largest contributors (e.g., cloud processes at JST and YRK). For production of the $PM_{2.5}$ mass
616 concentrations, emissions are the top contributor at urban sites whereas PM processes are the top
617 contributor at rural sites. Other processes such as vertical and horizontal transport may also be
618 important or even dominate at some sites (e.g., at GRSM and OLY). The important processes to the
619 loss of $PM_{2.5}$ mass concentrations include horizontal transport at urban and some rural sites (e.g., at
620 JST, LAX, YRK, and GRSM), and vertical transport at some rural sites (e.g., PSU and OLY). For
621 $PM_{2.5}$ surface area concentrations, important processes include emissions or PM processes for its
622 production at all sites except at GRSM where vertical transport dominates and at OLY where both
623 PM processes and horizontal transport are equally important. Horizontal transport dominates their
624 loss at urban sites and some rural sites (e.g., at JST, LAX, YRK, and GRSM) and vertical transport

625 dominates their loss at some sites (e.g., OLY), and cloud processes are important loss processes at
626 some sites (e.g., GRSM, YRK, and PSU). Compared with urban and upwind locations, processes
627 contributing to $PM_{2.5}$ number, mass, and surface areas are relatively more complicated at rural/remote
628 and/or downwind locations (e.g., GRSM and OLY).

629 **4.2 Sensitivity Simulations**

630 Given current model deficiency in reproducing PM number concentrations and size
631 distributions, the sensitivity study here is focused on several major factors that likely affect PM
632 number concentrations and size distributions. In addition to homogeneous nucleation, several
633 atmospheric processes such as emission and dry deposition may be important to the predicted PM
634 number concentrations and size distributions, as shown in the above process analysis. Several
635 parameters that may affect PM number emission rates include the assumed initial size distributions
636 for PM emitted, the assumed emission fractions of PM-AIT and PM-ACC in total $PM_{2.5}$ emissions,
637 and the direct emission rates of PM mass. In CMAQ, a constant PM size distribution with d_v of 0.03
638 μm and σ_g of 1.7 for PM-AIT and d_v of 0.3 μm and σ_g of 2.0 for PM-ACC is assumed based on
639 Whitby (1978) to calculate the emission rates for PM number and second moment (i.e., surface area),
640 E_{number} and $E_{surface}$ (Binkowski and Roselle, 2003). The values of d_v and σ_g may vary with regions of
641 applications that may have different characteristics of emission and meteorology. In this study, they
642 can be derived from the measured 24-hr average PM size distribution by assuming a lognormal
643 distribution which is a plausible assumption for most measurements of Aitken- and accumulation-
644 mode PM size distributions. Based on the ARIES measurements at JST, Atlanta, GA during June 12-
645 28, the derived values of d_v and σ_g are in the range of 0.0771-0.0925 μm and 2.195-2.6543,
646 respectively, for PM-AIT and 0.285-0.5075 μm and 1.5358-1.7922, respectively, for PM-ACC. The
647 17-day average values of d_v of 0.0903 μm and σ_g of 2.452 for PM-AIT and d_v of 0.3981 μm and σ_g of
648 1.6778 for accumulation-mode PM are used in the first sensitivity simulation (referred to as the
649 simulation "Initsize"). Similar sensitivity studies by adjusting the emission size distributions used in

650 CMAQ were conducted by Park et al. (2006) and Elleman and Covert (2010). For emission fractions,
651 CMAQ assumes that 99.9% of $PM_{2.5}$ emissions are in PM-ACC for organic and elemental carbon
652 (0.1% in PM-AIT). For other species such as sulfate and other inorganic aerosols, it assumes 100% in
653 PM-ACC (Binkowski and Roselle, 2003). This assumption is based on a field study of on-road
654 emissions of diesel soot conducted by the U.S. EPA (Francis S. Binkowski, the University of North
655 Carolina at Chapel Hill, 2005, personal communication) and may not be applicable for emissions of
656 all other $PM_{2.5}$ compositions. A sensitivity simulation (referred to as the simulation "Emisfrac") is
657 conducted to investigate this uncertainty. The observed volume concentrations of PM-AIT during
658 ARIES account for 0.5-14.2% of observed total volume concentrations of PM_2. The emission
659 fractions of Aitken- and accumulation-mode PM are therefore assumed to be 10% and 90%,
660 respectively, in this sensitivity simulation. P. Liu et al. (2010a) evaluated the model performance of
661 CMAQ using observed $PM_{2.5}$ concentrations for the same episode and found that $PM_{2.5}$
662 concentrations were underpredicted by 10.2-39.0% at various network sites. The concentrations of
663 NO_3^-, BC, and OC were underpredicted by 22.2-77.8%, 34.4-54.9%, and 24.9-58.6%, respectively,
664 and those of SO_4^{2-} were overpredicted by 17.8-20.1%, those of and NH_4^+ were overpredicted by 8.1-
665 24.2% at rural and remote sites but underpredicted by 20.6% at urban and suburban sites over the
666 southeastern U.S. By comparing with a more advanced NH_3 inventory, P. Liu et al. (2010b) reported
667 that the NH_3 emissions based on the NEI v3 used in this study were lower by 25.5% on average
668 domain-wide and an emission adjustment factor of 1.2551 was therefore applied to total NH_3
669 emission in their sensitivity simulations. Uncertainties also exist in the emissions of primary PM
670 species such as BC and OM (Zhang et al., 2006), which may have contributed to the discrepancies
671 between observed and simulated PM species for this episode. In the 3rd sensitivity simulation, the
672 emissions of primary PM species are therefore adjusted (i.e., increase by 50% for BC and by 40% for
673 OC and NO_3^-, and decrease by -20% for SO_4^{2-}) and the emissions of NH_3 are also increased by
674 25.51% (referred to as simulation "Emisadj"). In the 4th sensitivity simulation, dry deposition

675 velocities for $PM_{2.5}$ number and surface area are reduced by 20% (referred to as simulation
676 "Lowdepo"). The selection of such a perturbation is based on several considerations. First, no direct
677 measurements of dry deposition velocities for $PM_{2.5}$ number and surface area are available and one
678 must make some assumptions in selecting the value and direction of the perturbation. Second, the dry
679 deposition fluxes of PM number and surface area concentrations are assumed to be controlled by the
680 same processes as PM mass concentrations and the same set of equations is used to calculate dry
681 deposition fluxes of PM mass, number, and surface area concentrations in CMAQ. It is therefore
682 reasonable to assume that the uncertainties in dry depositions of PM number and surface area are the
683 same as or similar to those of PM mass concentrations. Third, X.-H. Liu et al. (2010b) and Olsen et
684 al. (2010) evaluated simulated dry deposition fluxes of several PM species against the calculated
685 values from CASTNET that are based on meteorological measurements and the predictions of the
686 Multilayer Model for a summer episode in the southeastern U.S. and found that CMAQ
687 underpredicted the dry deposition fluxes of PM species by 80-98%. Fourth, P. Liu et al. (2010 b)
688 conducted sensitivity simulations by changing dry deposition velocity of sulfate by 20% and those of
689 several PM precursors such as SO_2, HNO_3, and NH_3 by 20-50% for the same June 12-28, 1999 SOS
690 episode and found that a perturbation of 20% or larger is needed to predict a sizeable change (i.e., >
691 1-3%) in the simulated PM mass concentrations. Finally, simulated PM number and surface areas
692 from the baseline simulation in this study are underpredicted and using reduced dry deposition
693 velocities may help improve the model predictions. In the 5th sensitivity simulation, all
694 aforementioned changes are combined to estimate the net effects of above changes (referred to as
695 simulation "Combined"). In all five sensitivity simulations, the power law nucleation
696 parameterization of Sihto et al. (2006) is used, and the results from those sensitivity simulations are
697 compared with the baseline simulation with the Sihto et al. (2006) parameterization (i.e., SI06).

698 Figures 11, 12, and 13 show the times series plots of the predicted PM number, volume, and
699 surface areas, respectively, for Aitken- and accumulation-mode from the baseline simulation (i.e.,

700 SI06) and the five sensitivity simulations. The observations for both modes are also plotted for
701 comparison. Compared with baseline results, adjusting initial size distribution used in calculating PM
702 number and surface area emission rates gives higher number and surface area but lower volume
703 predictions for PM-AIT (the changes are 34.4%, -2.5%, and 5.4%, respectively on average over
704 hourly predictions on June 14-28) and slightly higher volume predictions for PM-ACC (by 0.1% on
705 average over hourly predictions on June 14-28) but lower number and surface area predictions for
706 PM-ACC (by -65.6% and -20.0%, respectively, on average over hourly predictions on June 14-28).
707 Increasing the emission fraction for PM-AIT from 0.1% to 10% further increases the predicted
708 number, volume, and surface area significantly (by factors of 3.2, 9.9, and 7.9, respectively, on
709 average over hourly predictions on June 14-28) but has little effect on those for PM-ACC (-2.2%, -
710 1.1%, and -1.1% for predicted number, volume, and surface area, respectively). This indicates that
711 the PM-AIT predictions are sensitive to the changes in both the emission fractions and the initial size
712 distribution used in this study, whereas the PM-ACC number and surface area predictions are more
713 sensitive to the changes in the initial size distribution than those in the emission fractions used, and
714 the PM-ACC volume predictions are relatively insensitive to changes in both parameters. The
715 simulated impact of adjusting initial size distribution of emissions on simulated PM number
716 concentrations is fairly consistent with that reported by Park et al. (2006) and Elleman and Covert
717 (2010). Adjusting the emissions of NH_3, BC, and primary OM species decreases PM-AIT number
718 concentrations by -2.7% but increases its volume and surface area concentrations by 4.7% and 3.3%,
719 respectively. It increases PM-ACC number, volume, and surface area concentrations by 8.8%, 8.5%,
720 and 7.9%, respectively. The relatively-small net increase in volume concentrations in responses to a
721 moderate-to-large increase in the emissions of NH_3, BC, and primary OM indicates that the PM mass
722 concentrations at JST may be dominated by other primary PM such as other unknown inorganic
723 aerosols and other secondary PM such as secondary organic aerosols and/or uncertainties in
724 meteorological factors (e.g., mixing height and temperature) may be a dominant factor for PM

725 concentrations. Reducing dry deposition velocity by 20% for PM number and surface areas for both
726 modes slightly increases PM-AIT and PM-ACC number concentration (by 1.2% and 0.9%,
727 respectively), PM-ACC volume concentration (0.005%, respectively), and PM-AIT and PM-ACC
728 PM surface area concentration (by 0.5% and 0.6%, respectively), but it slightly decreases the PM-
729 AIT volume concentration (by -0.5%). The simulation that combines all above changes increases the
730 number, volume, and surface area concentrations of PM-AIT by 56.7%, 67.6%, and 88.3%,
731 respectively. It also increases the surface area of PM-ACC by 6.9% but decreases its number and
732 volume concentrations by -63.9% and -15.0%, respectively. Among the five sensitivity simulations,
733 the simulations Initsize and Combined give the closer agreement to the observed temporal variations
734 for number, volume, and surface area predictions for PM-AIT but they both underpredict number and
735 volume concentrations of PM-ACC.

736 Tables 1(a) to 1(c) show the statistical measures for predicted total number, volume, and
737 surface area from the five sensitivity simulations. The predicted total $PM_{2.5}$ number concentration
738 changes from ~30000 cm^{-3} for the baseline simulation to ~38000, ~52000, ~29000, ~30000, and
739 ~44000 cm^{-3}, respectively, for simulations Inisize, Emisfrac, Emisadj, Lowdry, and Combined. The
740 increases in Initsize and Emisfrac are compensated by decreases in Emisadj in the simulation
741 Combined, resulting in the closest agreement to the observed number concentration of 43275 cm^{-3}
742 (changing the NMB from -31.7% to 1.6%). Reducing dry deposition velocity by 20% has little
743 effect on the total PM number predictions. While the changes in the simulations Initsize, Emisfrac,
744 and Lowdepo have little impact on volume concentrations, adjusting emissions in Emisadj and
745 Combined slightly improves them, changing the NMB value from -40% to -35%. The changes in
746 initial size distributions in Initsize and Combined decrease total surface areas (changing NMBs from -
747 36.6% to -48.4% and -39.2%, respectively), and the changes in the simulations Emisfrac and Emisadj
748 increase them (change NMBs from -36.6% to -28.9% and -31.5%, respectively). Tables 2(a) to 2(c)
749 show statistical measures for size-resolved number predictions from the five sensitivity simulations.

750 Both simulations Initsize and Combined improve the size-resolved number predictions over
751 segregated size sections, changing NMBs from -25.3% to -7.3% and 11.5%, respectively. The
752 simulation Emisfrac increases the NMB from -25.3% to 34%. The changes in simulations Lowdepo
753 and Emisadj have little effects on the size-resolved number predictions.

754 **5. Conclusions**

755 A total of 11 nucleation parameterizations are evaluated in 3-D CMAQ using available
756 measurements from ARIES to assess their appropriateness in reproducing number concentrations and
757 size distributions of $PM_{2.5}$ and the associated uncertainties. Among all parameterizations tested,
758 Napari et al. (2002) gives the highest number concentrations (by up to the order of 10^6 cm^{-3}), Sihto et
759 al. (2006), Harrington and Kreidenweis (1998), and Kuang et al. (2008) also give high number
760 concentrations (by up to the order of 10^5 cm^{-3}), Pandis et al. (1994) and Fitzgerald et al. (1998) give
761 moderate number concentrations (by up to the order of 10^4 cm^{-3}), and Merikanto et al. (2007), Yu
762 (2006), Yu (2008), Kulmala et al. (1998), and Vehkamäki et al. (2002) predict the lowest number
763 concentrations (by up to the order of 10^3 cm^{-3}). The predicted number concentrations for Aitken-
764 mode PM at JST, Atlanta can vary by up to three orders of magnitude, and those for accumulation-
765 mode PM can vary by up to a factor of 3.2. Such a large variation is caused by differences in their
766 theoretical bases, mathematical formulations, different dependence of T, RH, and the ambient levels
767 of H_2SO_4 and NH_3, as well as other processes considered. Compared with the observed values, the
768 total PM number concentrations are significantly underpredicted by all parameterizations, with the
769 best predictions by Sihto et al. (2006) (NMB of -31.7%) and the worst predictions by Merikanto et al.
770 (2007) (NMB of -93.1%). SI06 also gives the closest agreement to the observed hourly PM number,
771 volume, surface area, and their size distributions at JST among all parameterizations tested, although
772 all the parameterizations fail to reproduce the observed temporal variations of PM number, volume,
773 surface area at JST, Atlanta, GA. NA02 gives a good agreement with observed number
774 concentrations but such a good agreement is questionable and warrants further investigations. KU08

775 and HK98 give better performance than the rest of parameterizations. These results obtained under
776 an urban polluted condition are fairly consistent with the evaluation results under conditions from
777 very clean to highly-polluted environments from the Part I paper. The simulations with different
778 nucleation parameterizations show large uncertainties in the predicted PM number concentrations and
779 size distributions that will affect model predictions of visibility, aerosol optical properties such as
780 aerosol optical depth (AOD), CCN, and CNDC, demonstrating a need to improve the model's
781 capability in reproducing the PM concentrations and size distributions. Although the current version
782 of CMAQ does not simulate AOD, CCN, and CNDC online, a version of it that is being coupled with
783 the Weather Research and Forecasting model as an online modeling system (Pleim et al., 2008),
784 however, will simulate those parameters that are very important to the accurate predictions of aerosol
785 direct and indirect effects on climate change through modifying atmospheric radiation budgets.
786 Process analysis shows that controlling processes are different for Aitken-mode vs.
787 accumulation-mode, number vs. mass (or volume) vs. surface areas, and urban/upwind locations vs.
788 rural/remote/downwind locations. At all sites, controlling processes for $PM_{2.5}$ number concentrations
789 are similar to those for Aitken-mode PM, and those for $PM_{2.5}$ mass concentrations are similar to those
790 for accumulation-mode PM. At urban/upwind locations, the production of Aitken-mode number is
791 dominated by PM processes (e.g., homogeneous nucleation) and vertical transport, and its loss is
792 dominated by dry deposition. Horizontal transport and/or cloud processes may play an important
793 role, depending on the meteorological characteristics of the sites. Emission dominates the production
794 of accumulation-mode PM number and the major loss processes may include horizontal transport and
795 cloud processes. Emission dominates the production of accumulation-mode mass concentrations;
796 horizontal transport dominates their losses. Dominant processes for surface areas are generally
797 similar to those for $PM_{2.5}$ number concentrations. At rural/remote and/or downwind locations,
798 vertical and horizontal transport are major production processes for Aitken-mode PM number; and its
799 loss is controlled primarily by PM processes such as coagulation. For accumulation-mode PM

800 number, major production processes may include vertical transport and major loss processes may
801 include cloud processes, horizontal transport, and PM processes. For Aitken- and accumulation-
802 mode mass concentrations, vertical transport and PM processes dominate their production and
803 horizontal transport and cloud processes may dominate their loss. For PM surface areas, vertical and
804 horizontal transport dominate production of Aitken-mode surface areas, and cloud processes and dry
805 deposition may dominate their loss. Vertical transport and PM processes dominate the production of
806 accumulation-mode surface areas and horizontal transport and cloud processes dominate their loss.
807
808 Sensitivity simulations provide the relative importance of the assumed initial PM size
809 distribution and several atmospheric processes such as emissions and dry deposition in simulating PM
810 number concentrations and size distributions, in addition to that of the homogeneous nucleation
811 parameterization. Among these processes and parameters, the PM number and size distribution
812 predictions are most sensitive to prescribed emission fractions of Aitken and accumulation-mode PM
813 and the assumed initial PM size distribution, and relatively insensitive to dry deposition and
814 adjustments in emissions of NH_3 and PM species in this study. A simulation that combines all
815 changes increases the predicted total $PM_{2.5}$ number concentration from ~30000 cm^{-3} for the baseline
816 simulation to ~44000 cm^{-3}, changing the NMB value from -31.7% to 1.6%.
817 Accurately simulating PM number concentrations and size distributions remain a major
818 challenge because of inaccuracies in primary PM emissions and the relative emission fractions of
819 Aitken- and accumulation-mode PM, large uncertainties in the parameterizations of homogeneous
820 nucleation used in 3-D air quality model and the numerical algorithms of other important processes in
821 determining PM number and mass concentrations such as coagulation and other gas-to-particle
822 conversion processes (e.g., diffusion, condensation, heterogeneous reactions), uncertainties associated
823 with important model parameters such as initial PM size distribution, uncertainties in the model
824 treatment of nanoparticle growth to the CCN size, as well as lack of measurements (e.g., the size

825 resolved number, mass, and surface area concentrations of PM and the corresponding concentrations
826 of gas precursors of secondary PM such as SO_2, NO_x, NH_3, H_2SO_4, HNO_3, and VOCs) at sites
827 representative of various ambient atmospheric meteorological and chemical conditions for
828 model/parameterization validation. Extra cautions are advised in selecting a homogeneous nucleation
829 parameterization since most parameterizations have not been rigorously tested for all ranges of
830 ambient conditions and the appropriateness of one parameterization cannot be determined solely
831 based on whether it gives a good agreement with observations. The model evaluation conducted
832 here is based on a horizontal grid resolution of 32-km and uses observational data at only one urban
833 location. Given large differences in the controlling processes for PM number, volume, and surface
834 area predictions between urban/upwind locations and non-urban/downwind locations, the
835 performance of various nucleation parameterizations against observations may vary, depending on
836 characteristics of emissions, meteorology, topography of those locations, as well as the grid
837 resolution used for model simulations. The evaluation results from the calculations in the Part I paper
838 and the 3-D model simulations in this paper are fairly consistent. They indicate that among the
839 current parameterizations that are based on binary, ternary, kinetic, and cluster-activated nucleation
840 theories, Sihto et al. (2006), Kuang et al. (2008), and Harrington and Kreidenweis (1998) perform
841 better in the polluted boundary layer than most other parameterizations. Although Napari et al.
842 (2002) also gives a good agreement with observations under a sulfate-rich urban environment, it
843 should not be continuously used because of several fundamental problems associated with this
844 parameterization. As discussed previously, CMAQ does not simulate the growth of nanoparticle to
845 the Aitken mode, which will introduce a large uncertainty. It is therefore important to develop such a
846 growth module and couple it with a nucleation parameterization to reduce the uncertainty and
847 improve the model's capability in simulating PM number concentrations and size distributions.

848 **Acknowledgements**

This work was supported by the NSF Award No. Atm-0348819, the NOAA Award No. NA03NES4400015 and the Memorandum of Understanding between the U.S. Environmental Protection Agency (EPA) and the U.S. Department of Commerce's National Oceanic and Atmospheric Administration (NOAA) and under agreement number DW13921548, and the National Research Initiative Competitive Grant no. 2008-35112-18758 from the USDA Cooperative State Research, Education, and Extension Service Air Quality Program at North Carolina State University. PHM was supported by NSF Award Number ATM-0506674. FY acknowledges support from NSF Award No. AGS-0942106. Thanks are due to Hanna Vehkamäki, University of Helsinki, Finland, for providing a corrected version of code for Merikanto et al. (2007) parameterization, Alan Hansen, EPRI, for permitting the use of the ARIES PM number and size distribution data for model evaluation, Prakash V. Bhave, the U.S. EPA, for helpful discussions during an early stage of this work, and Kai Wang, NCSU, for help in post-processing process analysis results. Although this work was reviewed by EPA and approved for publication, it does not necessarily reflect their policies or views.

References

Binkowski, F.S., and S.J. Roselle, (2003), Models-3 community multiscale air quality (CMAQ) model aerosol component (1. Model description, *J. Geophys. Res.*, 108, 4183, doi:10.1029/2001JD001409.

Blando, J.D., R.J. Porcja, T.H. Li, D. Bowman, P.J. Lioy, and B. Turpin (1998). Secondary formation and the Smoky Mountain organic aerosol: an examination of aerosol polarity and functional group composition during SEAVS, *Environ. Sci. and Techno.*, 32, 604–613.

Byun, D., and K.L. Schere (2006), Review of the Governing Equations, Computational Algorithms, and Other Components of the Models-3 Community Multiscale Air Quality (CMAQ) Modeling System. *Appl. Mech. Rev.*, 59, 51– 77.

Day, D.E., W.C. Malm, and S.M. Kreidenweis (1997). Seasonal variations in aerosol composition and acidity at Shenandoah and Great Smoky Mountains National Parks. *J. of the Air and Waste Manage. Asso.*, 47, 411–418.

Eisele, F.L., and P.H. McMurry (1997), Recent progress in understanding particle nucleation and growth, Phil. Trans. R. Soc. Land. B, 352, 191-201.

Elleman R. A., and D. S. Covert (2009a), Aerosol size distribution modeling with the Community Multiscale Air Quality modeling system in the Pacific Northwest: 1. Model comparison to observations, *J. Geophys. Res.*, 114, D11206, doi:10.1029/2008JD010791.

Elleman R. A., and D. S. Covert (2009b), Aerosol size distribution modeling with the Community Multiscale Air Quality modeling system in the Pacific Northwest: 2. Parameterizations for ternary nucleation and nucleation mode processes, *J. Geophys. Res.*, 114, D11207, doi:10.1029/2009JD012187.

Elleman, R. A., and D. S. Covert (2010), Aerosol size distribution modeling with the Community Multiscale Air Quality modeling system in the Pacific Northwest: 3. Size distribution of particles emitted into a mesoscale model, *J. Geophys. Res.*, 115, D03204, doi:10.1029/2009JD012401.

Fitzgerald, J. W., W. A. Hoppel, and F. Gelbard (1998), A one-dimensional sectional model to simulate multicomponent aerosol dynamics in the marine boundary layer. 1. Modal description, *J. Geophys. Res.*, 103, 16085-16102.

Gaydos, T. M., C. O. Stanier, and S. N. Pandis (2005), Modeling of in situ ultrafine atmospheric particle formation in the eastern United States, *J. Geophys. Res.*, 110, D07S12, doi:10.1029/2004JD004683.

Harrington, D. Y., and S. M. Kreidenweis (1998), Simulation of Sulfate Aerosol Dynamics. I. Model Description. *Atmos. Environ.*, 32, 1691-1700.

Jacobson, M. Z. (1999), Studying the effects of calcium and magnesium on size-distributed nitrate and ammonium with EQUISOLV II, *Atmos. Environ.*, 33, 3635-3649.

Jung, J. G., S. N. Pandis, and P. J. Adams (2008), Evaluation of nucleation theories in a sulfur-rich environment, *Aerosol Sci. and Technol.*, 42, 495-504, doi: 10.1080/02786820802187085.

Jung, J., C. Fountoukis, P. J. Adams, and S. N. Pandis (2010), Simulation of in situ ultrafine particle formation in the eastern United States using PMCAMx-UF, *J. Geophys. Res.*, 115, D03203, doi:10.1029/2009JD012313.

Kavouras, I.G., N. Mihalopoulos, and E.G. Stephanou (1998), Formation of atmospheric particles from organic acids produced by forests. *Nature*, 395, 683-686, 1998.

Kerminen, V. M., and M. Kulmala (2002), Analytical formulae connecting the ''real'' and the ''apparent'' nucleation rate and the nuclei number concentration for atmospheric nucleation events, *J. Aerosol Sci.*, 33(4), 609–622.

Korhonen, H., K. S. Carslaw, D. V. Spracklen, D. A. Ridley, and J. Ström (2008), A global model study of processes controlling aerosol size distributions in the Arctic spring and summer, *J. Geophys. Res.*, 113, D08211, doi:10.1029/2007JD009114.

Kulmala, M., A. Toivonen, J. M. Makela, and A. Laaksonen (1998), Analysis of the growth of nucleation mode particles observed in Boreal forest, *Tellus*, 50B, 449-462.

Kulmala, M., L. Pirjola, and J. M. Mäkelä (2000), Stable sulphate clusters as a source of new atmospheric particles, *Nature*, 404, 66–69, doi:10.1038/35003550.

Kulmala, M., L. Laakso, K. E. J. Lehtinen, I. Riipinen, M. Dal Maso, T. Anttila, V.-M. Kerminen, U. Hõrrak, M. Vana, and H. Tammet (2004a), Initial steps of aerosol growth, *Atmos. Chem. Phys.*, 4, 2553– 2560.

Kulmala, M., H. Vehkamäki, T. Petäjä, M. Dal Maso, A. Lauri, V.-M. Kerminen, W. Birmili, and P. H. McMurry (2004b), Formation and growth rates of ultrafine atmospheric particles: A review of observations, *J. Aerosol Sci.*, 35, 143– 176, doi:10.1016/j.jaerosci.2003.10.003.

Kuang, C., P. H. McMurry, A. V. McCormick, and F. L. Eisele (2008), Dependence of nucleation rates on sulfuric acid vapor concentration in diverse atmospheric locations, *J. Geophys. Res.*, 113, D10209, doi:10.1029/2007JD009253.

Kuang, C., P. H., McMurry, and A. V. McCormick (2009), Determination of cloud condensation nuclei production from measured new particle formation events, *Geophys. Res. Lett.*, 36, L09822, doi:10.1029/2009GL037584.

Kulmala M., A. Laaksonen, and L. Pirjola (1998), Parameterizations for sulphric acid/water nucleation rates, *J. Geophys. Res.*, 103, 8301-8308.

Liu, P., and Y. Zhang (2010a), Use of a Process Analysis Tool for Diagnostic Study on Fine Particulate Matter Predictions in the U.S. Part I: Model Evaluation Using Surface, Aircraft, and Satellite Data, *Atmos. Pollu. Res.*, in review.

Liu, P., Y. Zhang, S.C. Yu, and K. L. Schere (2010b), Use of a Process Analysis Tool for Diagnostic Study on Fine Particulate Matter Predictions in the U.S. Part II: Process Analyses and Sensitivity Simulations, *Atmos. Pollu. Res.*, in review.

Liu, X.-H., Y. Zhang, J. Xing, Q. Zhang, D. G. Streets, C. J. Jang, W.-X. Wang, and J.-M. Hao (2010a), Understanding of Regional Air Pollution over China using CMAQ - Part II. Process Analysis and Ozone Sensitivity to Precursor Emissions, *Atmos. Environ.*, in press.

Liu, X.-H., Y. Zhang, K. Olsen, W.-X. Wang, B. Do, and G. Bridgers (2010b), Responses of Future Air Quality to Emission Controls over North Carolina, Part I. Model Evaluation for Current-Year Simulations, *Atmos. Environ.*, in press.

Lucas, D. D., and H. Akimoto (2006), Evaluating aerosol nucleation parameterizations in a global atmospheric model, *Geophys. Res. Lett.*, 33, L10808, doi:10.1029/2006GL025672.

Malm, W.C. (1979), Considerations in the measurements of visibility, *J. Air Pollut. Control Assoc.*, 29, 1042-1052.

McMurry, P.H. (1980), Photochemical aerosol formation from SO_2: a theoretical analysis of smog chamber data. *J. Colloid Interface Sci.*, 78, 513-527.

MuMurry, P.H. (1983), New particle formation in the presence of an aerosol: rates, time scales, and sub-0.01 μm size distributions. *J. Colloid Interface Sci.*, 95, 72-80.

McMurry, P.H., K.S. Woo, R. Weber, D.-R. Chen, and D. Y. H. Pui (2000), Size distributions of 3-10 nm atmospheric particles: implications for nucleation mechanisms, *Phil. Trans. R. Soc.*, London, A358, 2625-2642.

McMurry, P.H., and K.S. Woo (2002), Size Distributions of 3–100-nm Urban Atlanta Aerosols: Measurement and Observations, *Journal of Aerosol Medicine*, 15 (2), 169-178.

McMurry, P., M. Fink, H. Sakurai, M. Stolzenburg, L. Mauldin, K. Moore, J. Smith, F. Eisele, S. Sjostedt, and D. Tanner (2005), A criterion for new particle formation in the sulfur-rich Atlanta atmosphere, *J. Geophys. Res.*, 110, D22S02, doi:10.1029/2005JD005901.

Merikanto, J., E. Zapadinsky, A. Lauri, and H. Vehkamäki (2007), Origin of the failure of classical nucleation theory: Incorrect description of the smallest clusters, *Phys. Rev. Lett.*, 98 (145702, doi:10.1103/PhysRevLett.98.145702.

Merikanto, J., D. V. Spracklen, G. W. Mann, S. J. Pickering, and K. S. Carslaw (2009a), Impact of nucleation on global CCN, *Atmos. Chem. Phys.*, 9, 8601-8616.

Merikanto, J., I. Napari, H. Vehkamäki, T. Anttila, and M. Kulmala (2009b), Correction to "New parameterization of sulfuric acid-ammonia-water ternary nucleation rates at tropospheric conditions", *J. Geophys. Res.*, 114, D09206, doi:10.1029/2009JD012136.

Napari, I., M, Noppel, H. Vehkamäki, and M. Kulmala (2002), Parameterization of ternary nucleation rates for H_2SO_4-NH_3-H_2O vapors. *J. Geophys. Res., 107,* 4381, doi:10.1029/2002JD002132.

Noppel, M., H. Vehkamäki, and M. Kulmala (2002), An improved model for hydrate formation in sulfuric acid-water nucleation, *J. of Chem. Physics*, *116*, 218-228.

O'Halloran, T.L., J.D. Fuentes, D.R. Collins, M.J. Cleveland, and W.C. Keene (2009), Influence of air mass source region on nanoparticle events and hygroscopicity in central Virginia, U.S., *Atmos. Environ.*, 43, 3586–3595.

Olsen, K., Y. Zhang, S.-Y. Wu, W. Robarge, and J. Walker (2010), Fine Scale Modeling of Agricultural Air Quality over the Southeastern United States, Part I. Application and Evaluation of Two Air Quality Models, *Atmos. Environ.*, in preparation.

Pandis, S.N., L.M. Russell, and J.H. Seinfeld (1994), The relationship between DMS flux and CCN concentration in remote marine regions, *J. Geophys. Res.*, 99, 16945-16957.

Park, S.-K., A. Marmur, S. B. Kim, D. Tian, Y. Hu, P. H. McMurry, and A. G. Russell (2006), Evaluation of fine particle number concentrations in CMAQ, *Aerosol Sci. Technol.*, *40*, 985–996, doi:10.1080/02786820600907353.

Pierce, J. R., and P. J. Adams (2007), Efficiency of cloud condensation nuclei formation from ultrafine particles, *Atmos. Chem. Phys*, 7, 1367–1379.

Pierce, J.R., and P.J. Adams (2009), Uncertainty in global CCN concentrations from uncertain aerosol nucleation and primary emission rate, *Atmos. Chem. Phys.*, 9, 1339–1356.

Pleim, J., D. Wong, R. Mathur, J. Young, T. Otte, R. Gilliam, F. Binkowski, and A. Xiu (2008), Development of the Coupled 2-way WRF-CMAQ system, oral presentation at the 2008 Annual CMAS Conference, Research Triangle Park, NC, Oct. 6-8.

Roth H., W. Jiang, D. Yin, and E. Giroux (2003), CMAQ nucleation algorithms and their impact on PM modeling results in the lower fraser valley, presented at the 2003 CMAS Models-3 User's Workshop: One Atmosphere, One Community, One Modeling System: Models-3. Research Triangle Park, NC, October 27-29.

Seinfeld, J. H., and S. N. Pandis (2006), Atmospheric Chemistry and Physics: From Air Pollution to Climate Change, 2nd ed., 1232 pp., John Wiley, New York.

Sihto, S., M. Kulmala, V. Kerminen, M. Dal Maso, T. Petäjä, I. Riipinen, H. Korhonen, F. Arnold, R. Janson, and M. Boy (2006), Atmospheric sulphuric acid and aerosol formation: Implications from atmospheric measurements for nucleation and early growth mechanisms, *Atmos. Chem. Phys.*, 6, 4079– 4091.

Smith, J. N., M. J. Dunn, T. M. VanReken, K. Iida, M. R. Stolzenburg, P. H. McMurry, and L. G. Huey (2008), Chemical composition of atmospheric nanoparticles formed from nucleation in Tecamac, Mexico: Evidence for an important role for organic species in nanoparticle growth, *Geophys. Res. Lett.*, 35, L04808, doi:10.1029/2007GL032523.

Smith, J.N., K. C. Barsanti, H. R. Friedli, M. Ehn, M. Kulmala, D. R. Collins, J. H. Scheckman,

B.J. Williams, and P. H. McMurry (2010), Observations of aminium salt formation in atmospheric nanoparticles and possible climatic implications, *Proceedings of National Academy of Sciences*, 107 (15), 6634-6639. doi: 10.1073/pnas.0912127107.

Spracklen, D. V., K. J. Pringle, K. S. Carslaw, M. P. Chipperfield, and G. W. Mann (2005), A global off-line model of size-resolved aerosol microphysics: I. Model development and prediction of aerosol properties, *Atmos. Chem. Phys.*, 5, 2227-2252.

Spracklen, D. V., K. S. Carslaw, M. Kulmala, V.-M. Kerminen, G. W. Mann, and S.-L. Sihto (2006), The contribution of boundary layer nucleation events to total particle concentrations on regional and global scales, *Atmos. Chem. Phys.*, 6, 5631-5648.

Spracklen, D. V., K. J. Pringle, K. S. Carslaw, G. W. Mann, P. Manktelow, and J. Heintzenberg (2007), Evaluation of a global aerosol microphysics model against size-resolved particle statistics in the marine atmosphere, *Atmos. Chem. Phys.*, 7, 2073-2090.

Spracklen, D. V., K. S. Carslaw, M. Kulmala, V.-M. Kerminen, S.-L. Sihto, I. Riipinen, J. Merikanto, G. W. Mann, M. P. Chipperfield, A. Wiedensohler, W. Birmili, and H. Lihavainen (2008), Contribution of particle formation to global cloud condensation nuclei concentrations, *Geophys. Res. Lett.*, 35, L06808, doi:10.1029/2007GL033038.

Van Loy, M., T. Bahadori, R. Wyzga, B. Hartsell, and E. Ederton (2000). The aerosol research and inhalation epidemiology study (ARIES): PM2.5 mass and aerosol component concentrations and sampler intercomparisons. *J. Air & Waste manage. Assoc.*, 50, 1446-1458.

Vehkamäki, H., M. Kulmala, I. Napari, K.E.J. Lehtinen, C. Timmreck, M. Noppel, and A. Laaksonen (2002), An improved parameterization for sulfuric acid-water nucleation rates for tropospheric and stratospheric conditions, *J. Geophys. Res.*, *107*, 4622, doi:10.1029/2002JD002184.

Wang, K., Y. Zhang, C. J. Jang, S. Phillips, and B.-Y. Wang (2009), Modeling Study of Intercontinental Air Pollution Transport over the Trans-Pacific Region in 2001 using the

Community Multiscale Air Quality (CMAQ) Modeling System, *J. Geophys. Res.*, 114, D04307, doi:10.1029/2008JD010807.

Wexler, A. S., F. W. Lurmann, and J. H. Seinfeld (1994), Modeling Urban and Regional Aerosols. I. Model Development, *Atmos. Environ. 28*, 531-546.

Woo, K. S. (2003), Measurement of atmospheric aerosols: Size distributions of nanoparticles, estimation of size distribution moments and control of relative humidity, PhD thesis, Department of Mechanical Engineering, University of Minnesota.

Woo, K.S., D.R. Chen, D.Y.H. Pui, and P.H. McMurry (2001), Measurement of Atlanta aerosol size distributions: observations of ultrafine particle events, *Aerosol Science and Technology*, 34, 75-87.

Yu, F. (2006), Effect of ammonia on new particle formation: A kinetic H_2SO_4-H_2O-NH_3 nucleation model constrained by laboratory measurements, *J. Geophys. Res.* (111, D1, doi:10.1029/2005JD005968.

Yu, F. (2007), Improved quasi-unary nucleation model for binary H_2SO_4-H_2O homogeneous nucleation, *J. Chem. Phys.*, 127, 054301.

Yu, F. (2008), Updated H2SO4-H2O binary homogeneous nucleation rate look-up tables, *J. Geophy. Res.*, 113, D24201, doi:10.1029/2008JD010527.

Yu, F., and G. Luo (2009), Simulation of particle size distribution with a global aerosol model: Contribution of nucleation to aerosol and CCN number concentrations, *Atmos. Chem. Phys.*, 9, 7691-7710.

Yu, F., G. Luo, T. S. Bates, B. Anderson, A. Clarke, V. Kapustin, B. Yantosca, Y.-X. Wang, and S.-L. Wu (2010), Spatial distributions of particle number concentrations in the global troposphere: Simulations, observations, and implications for nucleation mechanisms, *J. Geophys. Res.*, doi:10.1029/2009JD013473, in press.

Yu, S., R. L. Dennis, P. V. Bhave, and B. K. Eder (2004), Primary and secondary organic aerosols over the United States: estimates on the basis of observed organic carbon (OC) and elemental carbon (EC), and air quality modeled primary OC/EC ratios, *Atmos. Environ.*, *38*, 5257-5268.

Yu, S.C., B. Eder, R. Dennis, S.-H. Chu, and S. Schwartz (2006), New unbiased symmetric metrics for evaluation of air quality models, *Atmospheric Science Letter*, 7, 26-34.

Yu, S.-C., R. Mathur, K. Schere, D. Kang, J. Pleim, J. Young, D. Tong, G. Pouliot, S.A. McKeen, and S.T. Rao (2008), Evaluation of real-time PM forecasts and process analysis for PM formation over the eastern United States using the Eta-CMAQ forecast model during the 2004 ICARTT study, *J. Geophys. Res.*, 113, D06204, doi:10.1029/2007JD009226.

Zhang, R., I. Suh, J. Zhao, D. Zhang, E.C. Fortner, X. Tie, L.T. Molina, and M.J. Molina (2004), Enhanced atmospheric new particle formation by organic acids, *Science*, 304, 1487-1490.

Zhang, Y., 2008, Online Coupled Meteorology and Chemistry models: History, Current Status, and Outlook, *Atmospheric Chemistry and Physics,* 8, 2895-2932.

Zhang, Y., C. Seigneur, J.H. Seinfeld, M.Z. Jacobson, and F.S. Binkowski (1999), Simulation of aerosol dynamics), A comparative review of algorithms used in air quality models, *Aerosol Sci. Technol.*, 31, 487-514.

Zhang, Y., and M.Z. Jacobson (2005), *A Comparative Study of Nucleation Parameterizations for 3-D Atmospheric Models*, presentation at the 9th Atmospheric Sciences and Air Quality Conference (ASAAQ2005), San Francisco, CA, April 27-29.

Zhang, Y., K. Vijayaraghavan, and C. Seigneur (2005), Evaluation of three probing techniques in a three-dimensional air quality model, *J. Geophys. Res.*, 110, D02305, doi:10.1029/2004JD005248.

Zhang, Y., P. Liu, B. Pun, and C. Seigneur (2006), A Comprehensive Performance Evaluation of MM5-CMAQ for Summer 1999 Southern Oxidants Study Episode, Part III. Diagnostic and Mechanistic Evaluations, *Atmos. Environ,* 40, 4856-4873.

Zhang, Y., J.-P. Huang, D. K. Henze, and J. H. Seinfeld (2007), The Role of Isoprene in Secondary Organic Aerosol Formation on a Regional Scale, *J. Geophys. Res.,* 112, D20207, doi:10.1029/2007JD008675.

Zhang, Y., Y.-S. Chen, P. Pillai, and X.-Y. Dong (2009a), Sensitivity of Simulated Aerosol and Cloud Properties to Nucleation Parameterizations in 3-D Regional and Global Models, presentation at the 28th Annual Meeting of AAAR, October 26-30, 2009, Minneapolis, MN.

Zhang, Y., X.-Y. Wen, K. Wang, and K. Vijayaraghavan, and M.Z. Jacobson (2009b), Probing into Regional O_3 and PM Pollution in the U.S., Part II. An Examination of Formation Mechanisms through a Process Analysis Technique and Sensitivity Study, *J. Geophys. Res.*, 114, D22305, doi:10.1029/2009JD011900.

Zhang, Y., P. Liu, X.-H. Liu, B. Pun, C. Seigneur, M.Z. Jacobson, and W.-X. Wang (2010a), Fine Scale Modeling of Wintertime Aerosol Mass, Number, and Size Distributions in Central California, *J. Geophys. Res.*, in press.

Zhang, Y., P. H. McMurry, F. Yu, and M.Z. Jacobson, (2010b), A Comparative Study of Homogeneous Nucleation Parameterizations, Part I. Examination and Evaluation of the Formulations, *J. Geophys. Res.,* in review.

Table 1. Performance statistics for hourly $PM_{2.5}$ number, volume, and surface areas predicted by CMAQ with various nucleation parameterizations and by sensitivity simulations at the surface layer during June 14-28, 1999.

a. Number

	PA94	FI98	HK98	KU98	VE02	YU08	NA02	ME07	YU06	SI06	KU08	Initsize	Emisfrac	Emisadj	Lowdepo	Combined	Max_J
MeanObs	43275	43275	43275	43275	43275	43275	43275	43275	43275	43275	43275	43275	43275	43275	43275	43275	43275
MeanMod	5699	4704	21241	3289	3489	3163	26999	2996	3071	29562	17332	38052	51993	28958	29555	43952	584767
Data #	262	262	262	262	262	262	262	262	262	262	262	262	262	262	262	262	262
NMB, %	-86.8	-89.1	-50.9	-92.4	-91.9	-92.9	-37.6	-93.1	-92.7	-31.7	-59.9	-12.1	20.1	-33.1	-30.8	1.6	1251.3
NME, %	86.8	89.1	84.5	92.4	91.9	92.9	110.5	93.1	92.7	63.1	72.9	73.2	51.2	61.7	63.0	60.3	1251.3
NMBF	-6.6	-8.2	-1.0	-12.2	-11.4	-12.7	-0.6	-13.5	-13.1	-0.5	-1.50	-0.1	0.2	-0.5	-0.5	0.02	12.5
NMEF	6.6	8.2	1.7	12.2	11.4	12.7	1.8	13.5	13.1	0.9	1.82	0.8	0.5	0.9	0.9	0.6	12.5

b. Volume

	PA94	FI98	HK98	KU98	VE02	YU08	NA02	ME07	YU06	SI06	KU08	Initsize	Emisfrac	Emisadj	Lowdepo	Combined	Max_J
MeanObs	15.93	15.93	15.93	15.93	15.93	15.93	15.93	15.93	15.93	15.93	15.93	15.93	15.93	15.93	15.93	15.93	15.93
MeanMod	9.59	9.58	9.56	9.57	9.57	9.58	9.44	9.58	9.58	9.56	9.57	9.56	9.58	10.39	9.56	10.42	9.50
Data #	244	244	244	244	244	244	244	244	244	244	244	244	244	244	244	244	244
NMB,%	-39.8	-39.9	-40.0	-39.9	-39.9	-39.9	-40.7	-39.9	-39.9	-40.0	-39.9	-40.0	-39.8	-34.8	-40.0	-34.6	-40.4
NME,%	47.0	47.1	47.2	47.1	47.1	47.1	47.7	47.1	47.1	47.2	47.1	47.2	47.1	45.0	47.2	44.9	47.5
NMBF	-0.7	-0.7	-0.7	-0.7	-0.7	-0.7	-0.7	-0.7	-0.7	-0.7	-0.7	-0.7	-0.7	-0.5	-0.7	-0.5	-0.7
NMEF	0.8	0.8	0.8	0.8	0.8	0.8	0.8	0.8	0.8	0.8	0.8	0.8	0.8	0.7	0.8	0.7	0.8

c. Surface area

	PA94	FI98	HK98	KU98	VE02	YU08	NA02	ME07	YU06	SI06	KU08	Initsize	Emisfrac	Emisadj	Lowdepo	Combined	Max_J
MeanObs	309.8	309.8	309.8	309.8	309.8	309.8	309.8	309.8	309.8	309.8	309.8	309.8	309.8	309.8	309.8	309.8	309.8
MeanMod	187.3	180.7	194.5	163.3	165. 8	164.5	195.4	162.1	162.2	196.6	195.0	156.0	220.3	212.3	197.7	188.5	253.7
Data #	244	244	244	244	244	244	244	244	244	244	244	244	244	244	244	244	244
NMB,%	-39.5	-41.7	-37.2	-47.3	-46.5	-47.6	-36.9	-47.7	-46.9	-36.6	-37.1	-48.4	-28.9	-31.5	-36.2	-39.2	-18.1
NME,%	44.6	46.2	42.6	51.1	50.4	51.4	42.8	51.4	50.7	42.3	42.7	49.5	39.1	40.2	42.1	42.8	35.9
NMBF	-0.7	-0.7	-0.6	-0.9	-0.9	-0.9	-0.6	-0.9	-0.9	-0.6	-0.6	-0.9	-0.4	-0.5	-0.6	-0.6	-0.2
NMEF	0.7	0.8	0.7	1.0	0.9	1.0	0.7	1.0	1.0	0.7	0.7	1.0	0.6	0.6	0.7	0.7	0.4

[1] PA94, FI98, HK98, KU98, VE02, YU08, NA02, ME07, YU06, SI06, and KU08 denote Pandis et al. (1994), Fitzgerald et al. (1998), Harrington and Kreidenweis (1998), Kulmala et al. (1998), Vehkamäki et al. (2002), Yu (2008), Napari et al. (2002), Merikanto et al. (2007), Yu (2006), Sihto et al. (2006), and Kuang et al. (2008). Initsize, Emisfrac, Emisadj, Lowdepo, and Combined denote sensitivity simulations that use SI06 but with changes in either model input or process parameters.

[2] NMB, NME, NMBF, and NMEF denote normalized mean bias, normalized mean error, normalized mean bias factor, and normalized mean error factor, respectively. An NMBF value of -12.2 mean an underprediction by a factor of -13.2 (Yu et al., 2006).

Table 2. Performance statistics for size-resolved number, volume, and surface area size distributions predicted by CMAQ with various nucleation parameterizations and by sensitivity simulations at the surface layer during June 14-28, 1999.

a. Number

	PA94	FI98	HK98	KU98	VE02	YU08	NA02	ME07	YU06	SI06	KU08	Initsize	Emisfrac	Emisadj	Lowdepo	Combined	Max_J
MeanObs	1035.7	1035.7	1035.7	1035.7	1035.7	1035.7	1035.7	1035.7	1035.7	1035.7	1035.7	1035.7	1035.7	1035.7	1035.7	1035.7	1035.7
MeanMod	157.4	136.5	599.9	91.1	97.2	86.4	793.5	83.6	83.5	773.2	464.3	959.9	1387.5	766.0	783.9	1155.2	12599.5
Data #	585	585	585	585	585	585	585	585	585	585	585	585	585	585	585	585	585
NMB,%	-84.8	-86.8	-42.1	-91.2	-90.6	-91.9	-23.4	-91.9	-91.7	-25.3	-55.2	-7.3	34.0	-26.0	-24.4	11.5	1116.5
NME,%	90.7	91.3	82.1	92.9	92.5	93.0	85.7	93.5	92.8	68.1	78.4	70.2	126.8	69.5	68.2	91.8	1123.1
NMBF	-5.9	-6.6	-0.7	-10.4	-9.7	-11.0	-0.3	-11.4	-11.4	-0.3	-1.2	-0.1	0.3	-0.4	-0.3	0.1	11.2
NMEF	6.0	6.9	1.4	10.6	9.9	11.1	1.1	11.6	11.5	0.9	1.8	0.8	1.3	0.9	0.9	0.9	11.2

b. Volume

	PA94	FI98	HK98	KU98	VE02	YU08	NA02	ME07	YU06	SI06	KU08	Initsize	Emisfrac	Emisadj	Lowdepo	Combined	Max_J
MeanObs	0.46	0.46	0.46	0.46	0.46	0.46	0.46	0.46	0.46	0.46	0.46	0.46	0.46	0.46	0.46	0.46	0.46
MeanMod	0.24	0.24	0.26	0.24	0.24	0.25	0.25	0.23	0.25	0.256	0.26	0.26	0.26	0.28	0.26	0.28	0.24
Data #	585	585	585	585	585	585	585	585	585	585	585	585	585	585	585	585	585
NMB,%	-47.9	-48.0	-44.8	-49.1	-49.3	-45.8	-45.6	-49.6	-45.7	-44.7	-44.7	-44.4	-44.5	-40.1	-44.7	-39.6	-47.7
NME,%	66.5	67.0	61.7	71.3	69.1	70.0	60.4	72.1	69.0	61.3	61.5	68.0	61.5	59.9	61.0	67.0	57.9
NMBF	-0.9	-0.9	-0.8	-1.0	-1.0	-0.8	-0.8	-1.0	-0.9	-0.8	-0.8	-0.8	-0.8	-0.7	-0.8	-0.7	-0.9
NMEF	1.3	1.3	1.1	1.4	1.4	1.3	1.1	1.4	1.3	1.1	1.1	1.2	1.1	1.0	1.1	1.1	1.1

c. Surface area

	PA94	FI98	HK98	KU98	VE02	YU08	NA02	ME07	YU06	SI06	KU08	Initsize	Emisfrac	Emisadj	Lowdepo	Combined	Max_J
MeanObs	9.06	9.06	9.06	9.06	9.06	9.06	9.06	9.06	9.06	9.06	9.06	9.06	9.06	9.06	9.06	9.06	9.06
MeanMod	5.07	4.95	5.52	4.32	4.40	4.58	5.55	4.29	4.49	5.56	6.92	4.59	6.17	5.98	5.59	5.35	6.96
Data #	585	585	585	585	585	585	585	585	585	585	585	585	585	585	585	585	585
NMB	-44.0	-45.4	-39.1	-52.3	-51	-50.4	-38.8	-52.7	-49.5	-38.6	-23.6	-49.4	-31.8	-34.0	-38.3	-41.0	-23.1
NME	59.1	60.3	54.1	64.9	64	63.2	51.2	65.4	62.1	53.6	66.8	68.1	57.2	52.1	53.0	66.2	59.7
NMBF	-0.8	-0.8	-0.6	-1.1	-1.1	-1.0	-0.6	-1.1	-1.0	-0.6	-0.3	-1.0	-0.8	-0.5	-0.6	-0.7	-0.3
NMEF	1.1	1.1	0.9	1.4	1.3	1.2	0.8	1.4	1.3	0.9	0.9	1.4	0.8	0.8	0.9	1.1	0.8

[1] PA94, FI98, HK98, KU98, VE02, YU08, NA02, ME07, YU06, SI06, and KU08 denote Pandis et al. (1994), Fitzgerald et al. (1998), Harrington and Kreidenweis (1998), Kulmala et al. (1998), Vehkamäki et al. (2002), Yu (2008), Napari et al. (2002), Merikanto et al. (2007), Yu (2006), Sihto et al. (2006), and Kuang et al. (2008). Initsize, Emisfrac, Emisadj, Lowdepo, and Combined denote sensitivity simulations that use SI06 but with changes in either model input or process parameters.

[2] NMB, NME, NMBF, and NMEF denote normalized mean bias, normalized mean error, normalized mean bias factor, and normalized mean error factor, respectively. An NMBF value of -5.9 mean an underprediction by a factor of -6.9 (Yu et al., 2006).

Table 3. The 15-day average (June 14-28, 1999) changes in PM number, mass, and surface areas of Aitken- and accumulation-mode particles due to seven major atmospheric processes at JST, Atlanta, GA, Los Angeles (LAX), CA, and GRS, TN.

(a) Changes in PM number concentrations (cm^{-3} hr^{-1})

		Horizontal Transport	Vertical Transport	Emissions	Dry Deposition	PM processes	Cloud Processes	Mass Balance Adjustment
Aitken	JST	-2.2E+02	6.1E+01	1.5E+01	-1.4E+03	2.6E+03	-1.1E+03	-1.5E+01
	LAX	-3.9E+04	7.8E+02	1.8E+01	-4.8E+04	8.6E+04	-2.3E+01	-3.2E+02
	GRSM	3.3E+02	6.3E+02	2.9E-01	-9.3E+01	-1.0E+03	1.3E+02	1.0E+01
Accumulation	JST	-6.2E+01	-2.9E+00	1.0E+02	-3.8E+00	-7.0E+00	-3.0E+01	-4.3E-01
	LAX	-1.1E+02	1.4E+01	7.0E+01	-8.0E+00	3.2E+01	-5.3E-01	-1.1E+00
	GRSM	-7.3E+00	2.3E+01	1.5E+00	-2.1E+00	-6.0E+00	-1.2E+01	2.1E+00

(b) Changes in PM mass concentrations (μg m^{-3} hr^{-1})

		Horizontal Transport	Vertical Transport	Emissions	Dry Deposition	PM processes	Cloud Processes	Mass Balance Adjustment
Aitken	JST	-4.6E-05	-1.1E-05	1.3E-06	-6.4E-06	1.0E-04	-3.9E-05	-2.4E-06
	LAX	-2.4E-05	1.1E-05	1.5E-06	-9.3E-07	1.2E-05	-7.1E-08	-3.6E-07
	GRSM	-1.0E-04	7.8E-05	2.1E-08	-6.6E-06	6.9E-05	-6.2E-05	1.5E-05
Accumulation	JST	-4.5E-03	-4.0E-04	3.5E-03	-8.0E-05	1.9E-03	-3.9E-04	-2.2E-05
	LAX	-3.5E-03	3.8E-04	2.4E-03	-5.9E-05	7.9E-04	4.2E-05	-6.1E-05
	GRSM	-1.1E-03	1.1E-03	5.3E-05	-7.7E-05	5.8E-04	-6.3E-04	1.3E-04

(c) Changes in PM surface areas (μm^2 cm^{-3} hr^{-1})

		Horizontal Transport	Vertical Transport	Emissions	Dry Deposition	PM processes	Cloud Processes	Mass Balance Adjustment
Aitken	JST	-1.7E-02	-2.5E-02	1.4E-02	-9.9E-02	4.6E-01	-3.5E-01	-4.7E-03
	LAX	-2.1E+00	1.6E-01	1.6E-02	-1.7E+00	3.7E+00	-2.9E-03	-2.1E-02
	GRSM	7.0E-02	2.9E-01	2.7E-04	-7.8E-02	2.9E-02	-3.6E-01	3.4E-02
Accumulation	JST	-3.9E+00	-2.4E-01	4.3E+00	-1.0E-01	1.1E+00	-1.2E+00	-2.8E-02
	LAX	-4.3E+00	4.1E-01	2.9E+00	-1.1E-01	1.0E+00	-6.6E-03	-5.8E-02
	GRSM	-1.0E+00	1.2E+00	6.4E-02	-7.5E-02	3.9E-01	-7.0E-01	1.5E-01

List of Figures for the Part II Paper

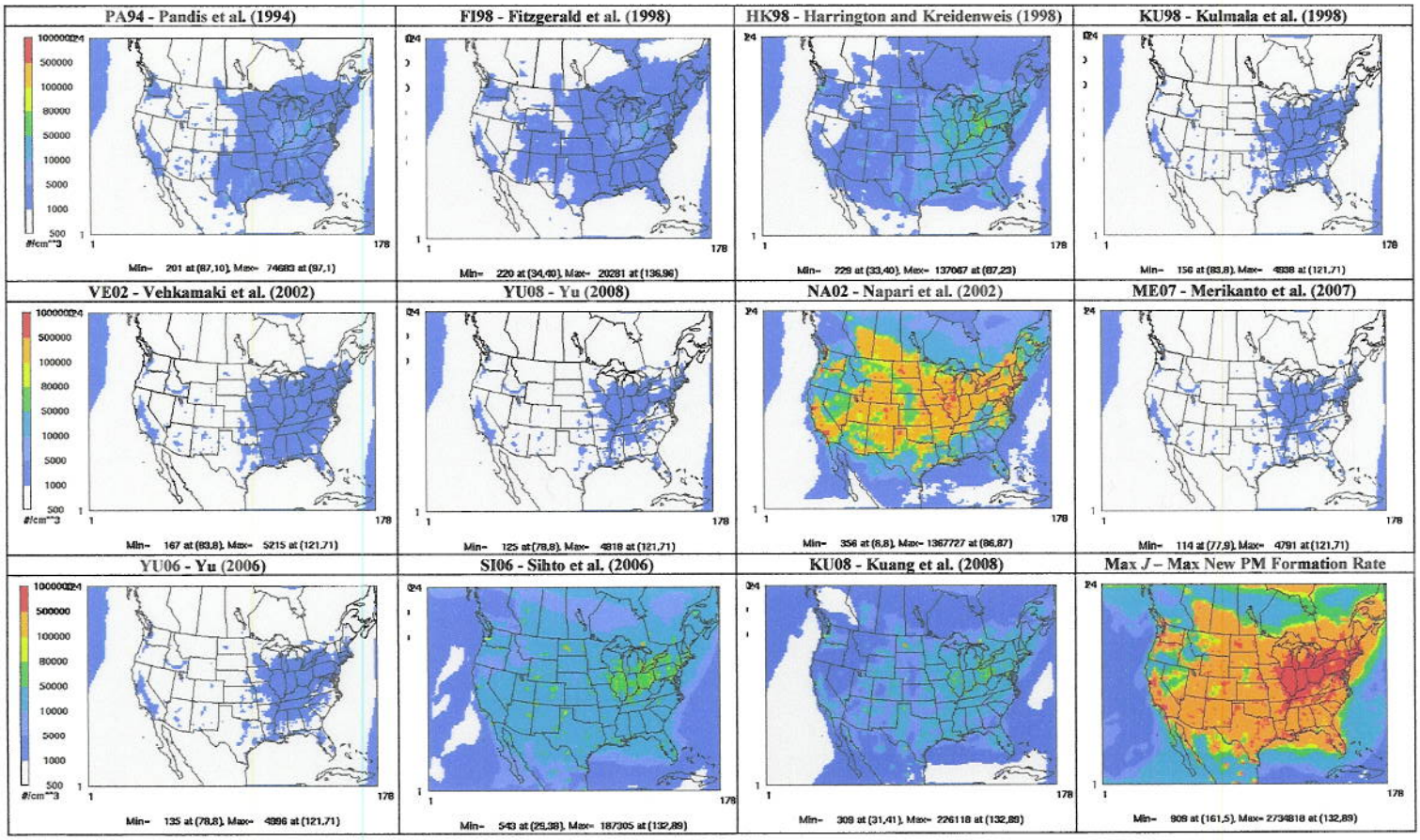

Figure 1. The 15-day average (June 14-28, 1999) hourly total number concentrations of $PM_{2.5}$ predicted with the 11 nucleation parameterizations. Max *J* represents the maximum nucleation rates for particles with diameter of 2 nm defined in Part I (Zhang et al., 2010).

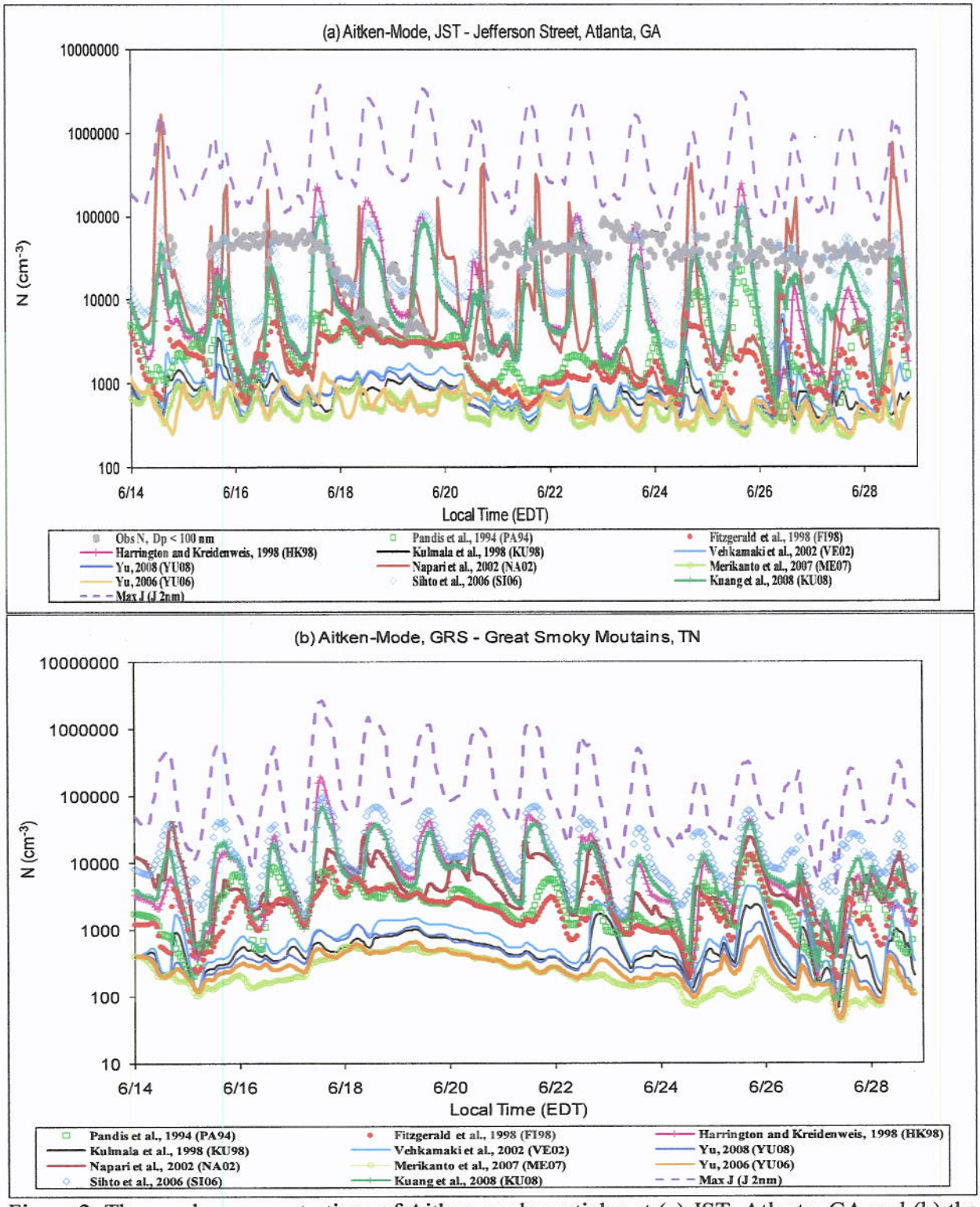

Figure 2. The number concentrations of Aitken-mode particles at (a) JST, Atlanta, GA and (b) the Great Smoky Mountains (GRS), TN predicted with the 11 nucleation parameterizations. The observational data at JST are obtained for particles with diameter $\leq$ 100 nm from ARIES. No observational data are available at GRS.

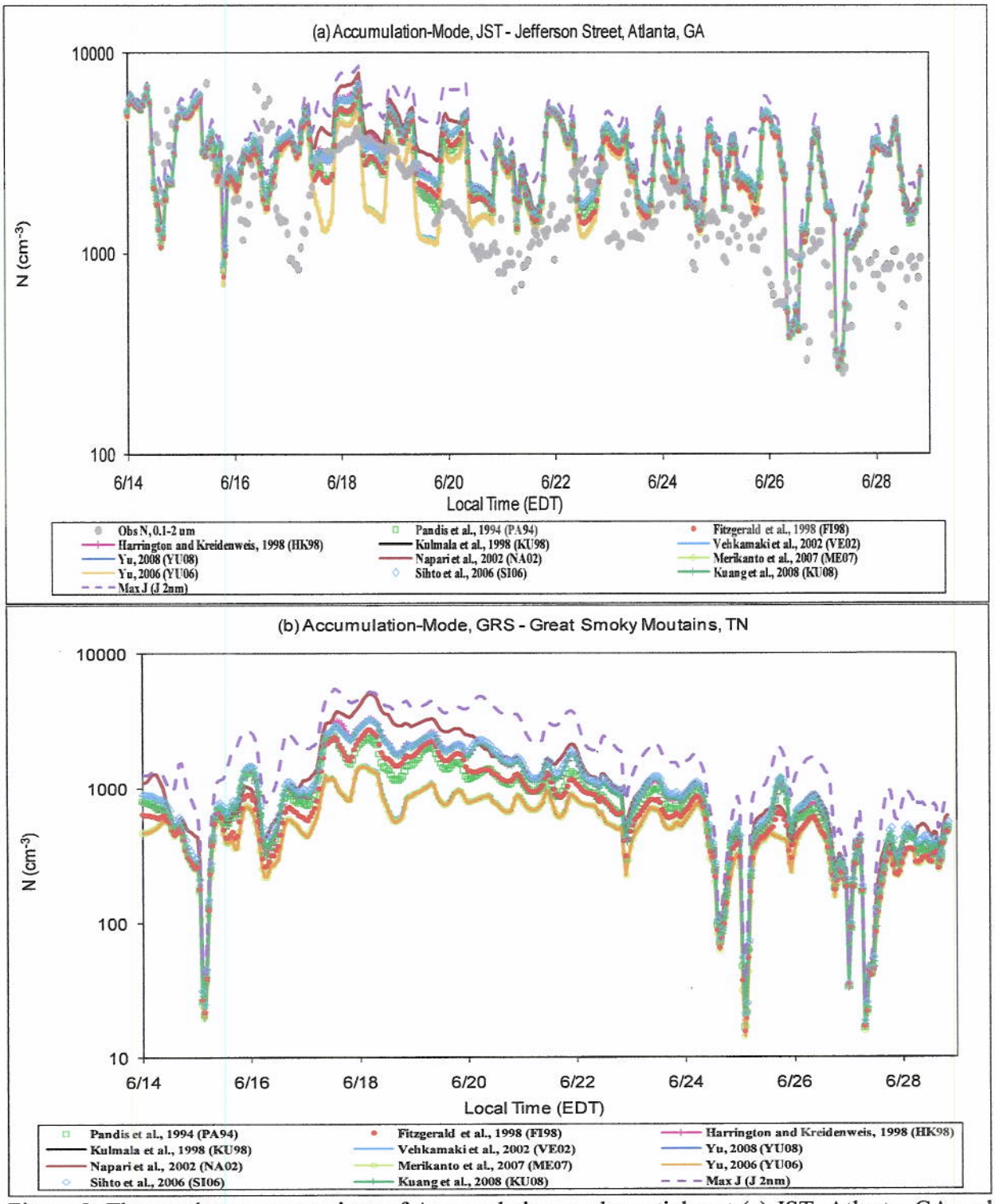

Figure 3. The number concentrations of Accumulation-mode particles at (a) JST, Atlanta, GA and (b) the Great Smoky Mountains (GRS), TN predicted with the 11 nucleation parameterizations. The observational data at JST are obtained for particles with diameter $\leq$ 100 nm from ARIES. No observational data are available at GRS.

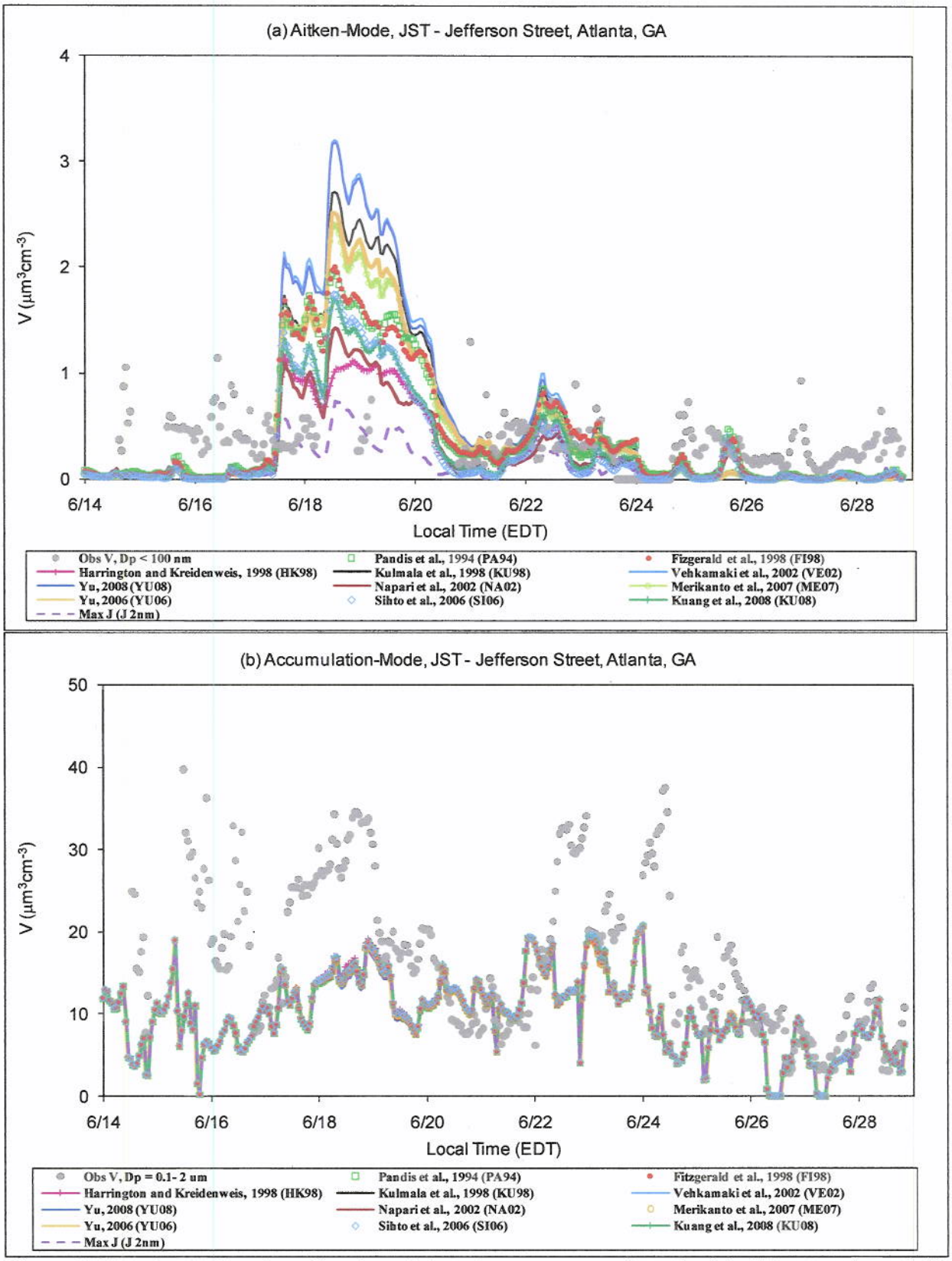

Figure 4. The observed and predicted particle volume concentrations for (a) Aitken-mode, and (b) Accumulation-mode at JST, Atlanta, GA.

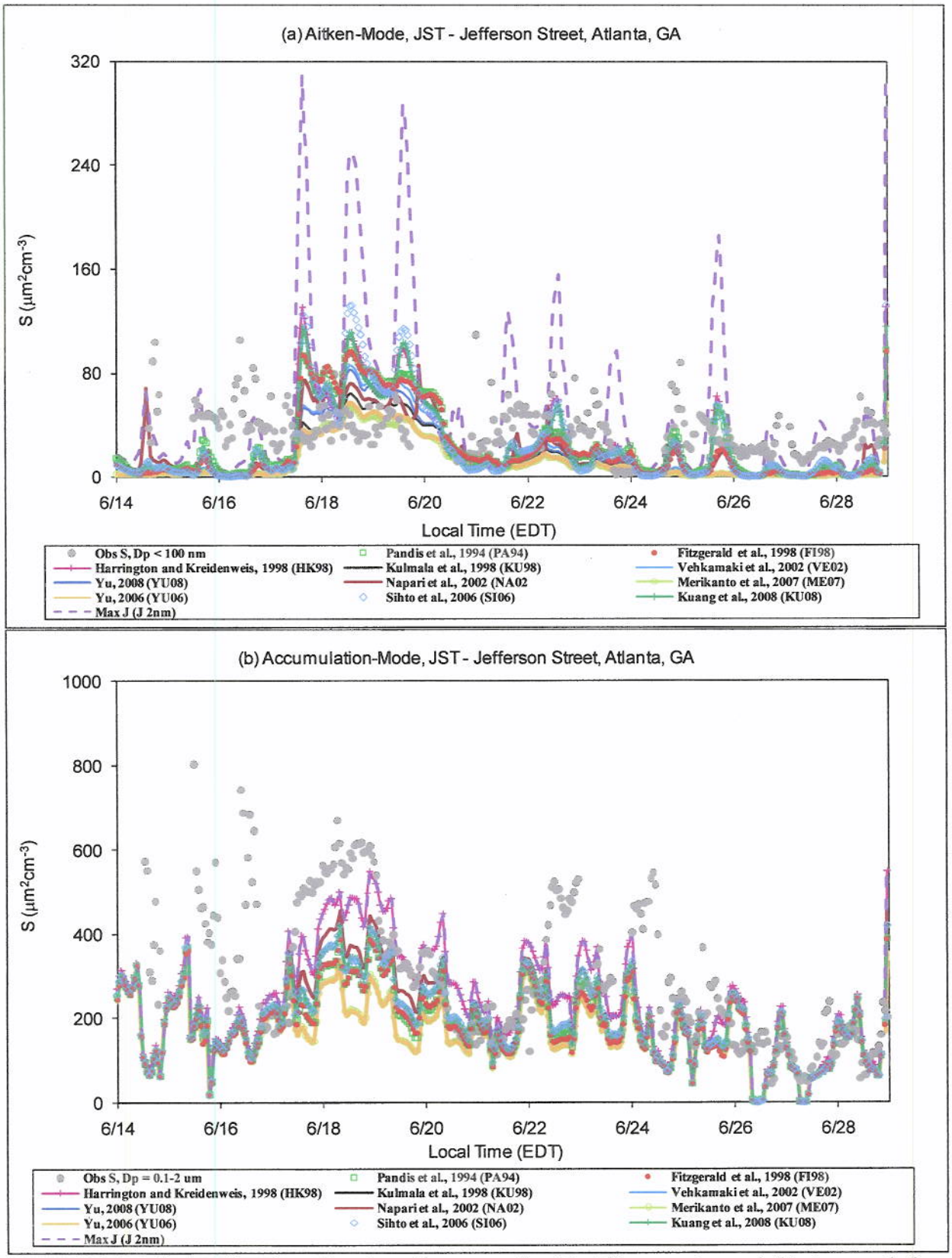

Figure 5. The observed and predicted surface areas for (a) Aitken-mode, and (b) Accumulation-mode at JST, Atlanta, GA.

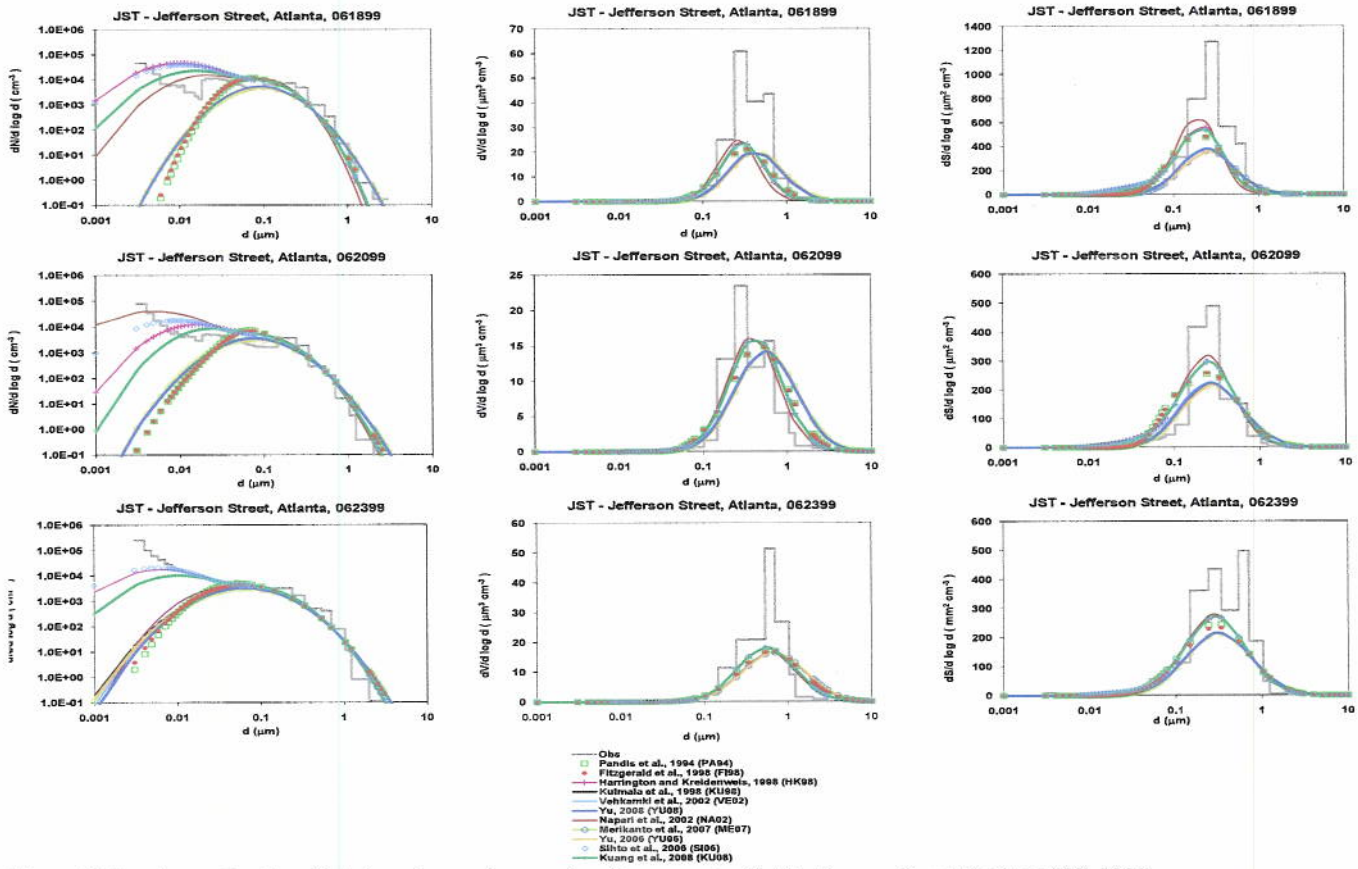

Figure 6. The observed and predicted number, volume and surface area size distributions on June 18, 20, and 23, 1999.

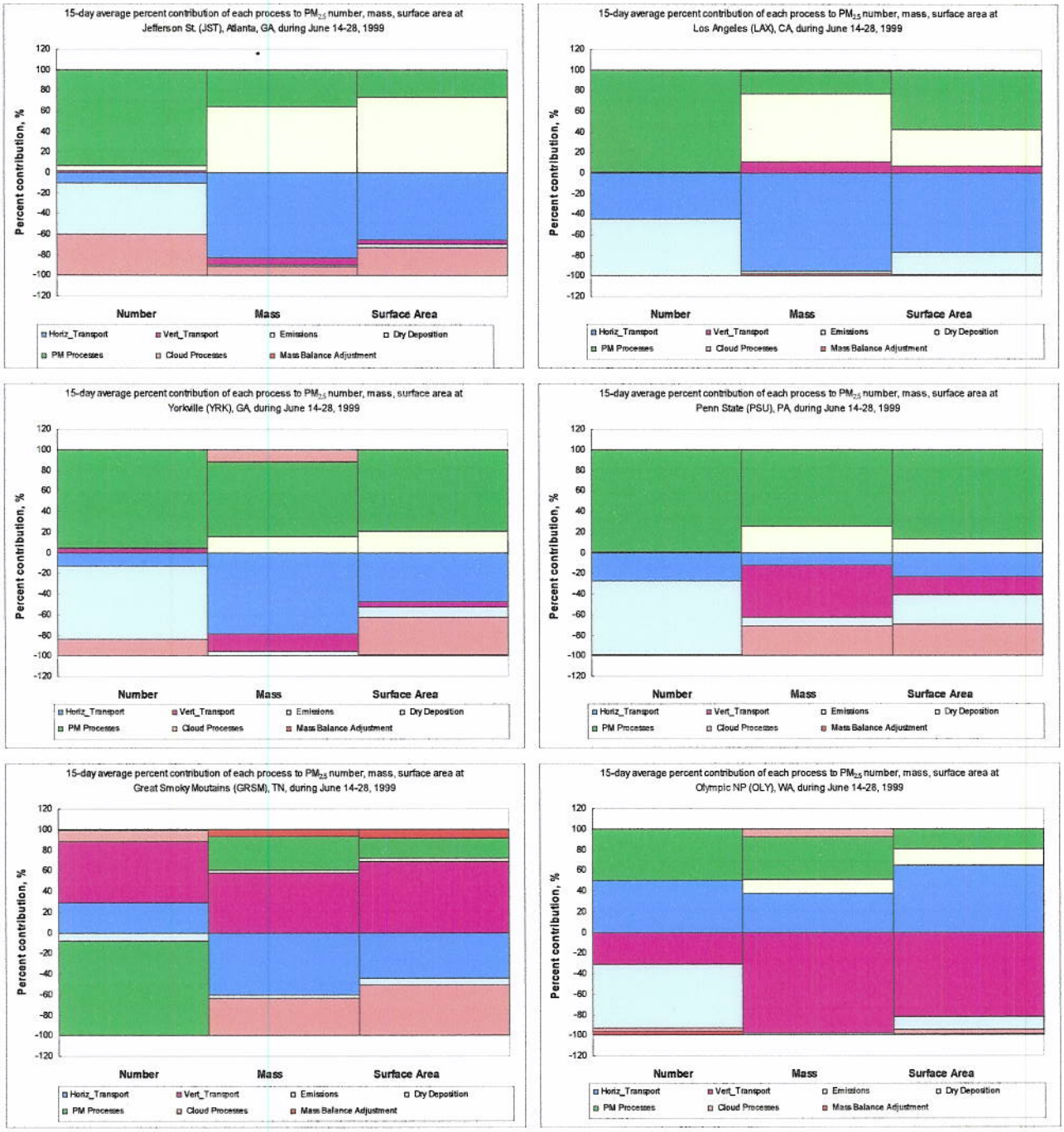

Figure 7. The 15-day average (June 14-28, 1999) percentage contributions of each process to number, mass, and surface area concentrations of $PM_{2.5}$ (Aitken- and accumulation-mode PM) at two urban sites ((a) JST and (b) LAX), two rural sites ((c) Yorkville (YRK), GA and (d) Penn State (PSU), PA), and two remote sites ((e) GRSM and (f) Olympic National Park (OLY)).

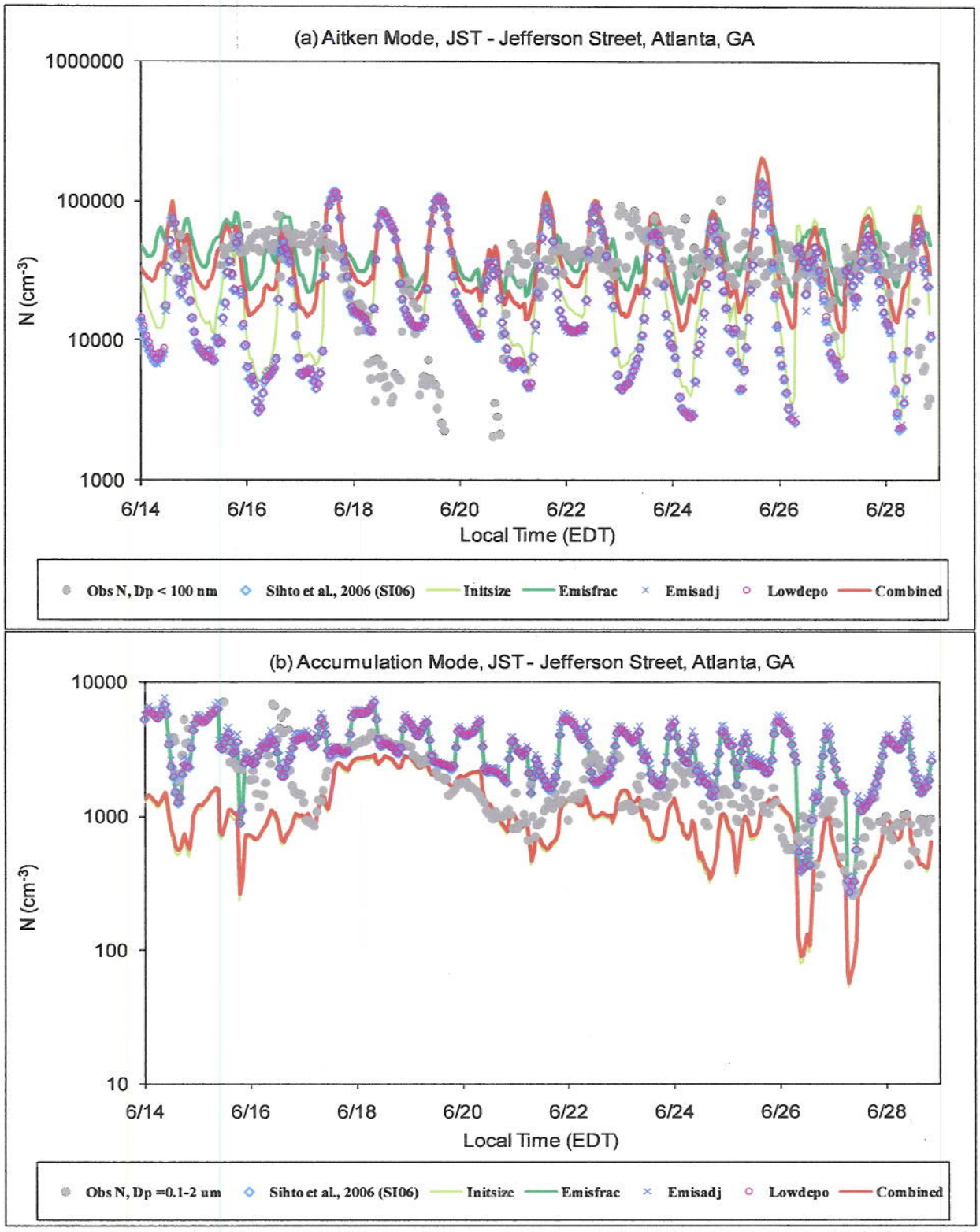

Figure 8. The predicted hourly PM number concentrations for Aitken- and accumulation-mode from the baseline simulation (i.e., SI06) and the five sensitivity simulations (i.e., Initisize, Emisfrac, Emisadj, Lowdepo, and Combined) during June 14-28, 1999.

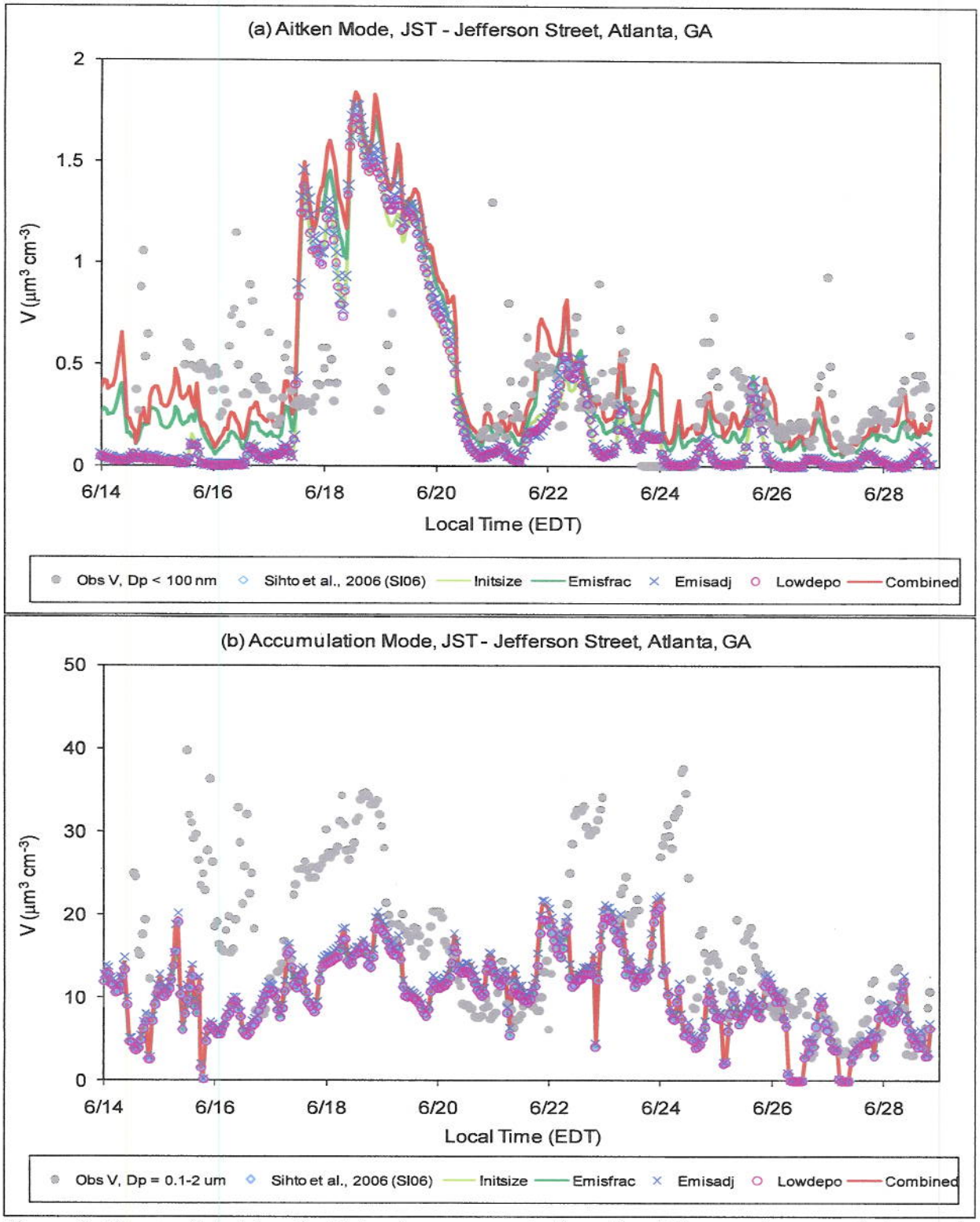

Figure 9. The predicted hourly PM volume concentrations for Aitken- and accumulation-mode from the baseline simulation (i.e., SI06) and the five sensitivity simulations (i.e., Initisize, Emisfrac, Emisadj, Lowdepo, and Combined) during June 14-28, 1999.

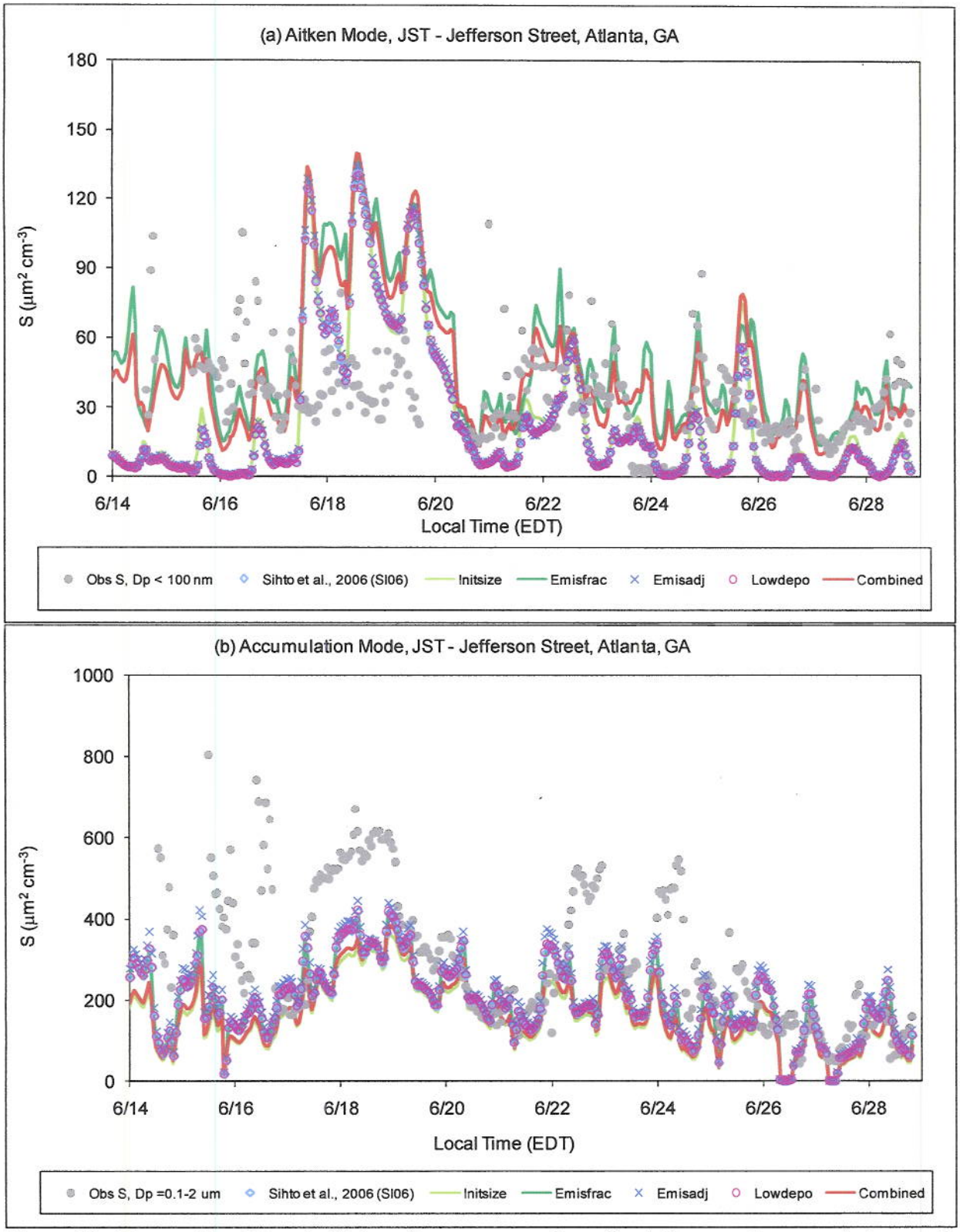

Figure 10. The predicted hourly PM surface concentrations for Aitken- and accumulation-mode from the baseline simulation (i.e., SI06) and the five sensitivity simulations (i.e., Initisize, Emisfrac, Emisadj, Lowdepo, and Combined) during June 14-28, 1999.